Received 00th January 20xx,
Accepted 00th January 20xx

DOI: 10.1039/x0xx00000x

Supporting information

The influence of trinuclear complexes on the light induced hydrogen production

Helena Roithmeyer[a], Richard Pehn[a] , Johann Pann[a], Wolfgang Viertl[a], Benedikt Trübenbacher[a], Julian Dutzler[a], Holger Kopacka[a], Thomas Müller[b] and Peter Brüggeller [a,]

[a.] *University of Innsbruck, Centrum for Chemistry and Biomedicine, Institute of General, Inorganic and Theoretical Chemistry, Innrain 82, 6020 Innsbruck, Austria. e-mail: Peter.Brueggeller@uibk.ac.at; mobile: +43 664 3461922.*

[b.] *University of Innsbruck, Centrum for Chemistry and Biomedicine, Institute of Organic Chemistry, Innrain 82, 6020 Innsbruck, Austria.*

Contents

1. Experimental procedures

1.1. General experimental

All syntheses were accomplished using standard Schlenk technique under inert gas argon atmosphere with degassed and extra dry solvents. All solvents and reactants were purchased from Sigma-Aldrich. NMR spectra were recorded on a Bruker Avance DPX 300 NMR-spectrometer. ^{1}H NMR spectra were referenced to the solvents signal. ^{31}P spectra are referenced on H_3PO_4. The IR/ATR-spectra were performed on a Bruker Platinum-ATR. Bis(diorthoanisyl)phosphine was synthesised according to literature.[1] 1,3,5-tris(amino-methyl)benzene was synthesised according to literature-known procedures.[2,3]

1.2. Syntheses and Characterisation

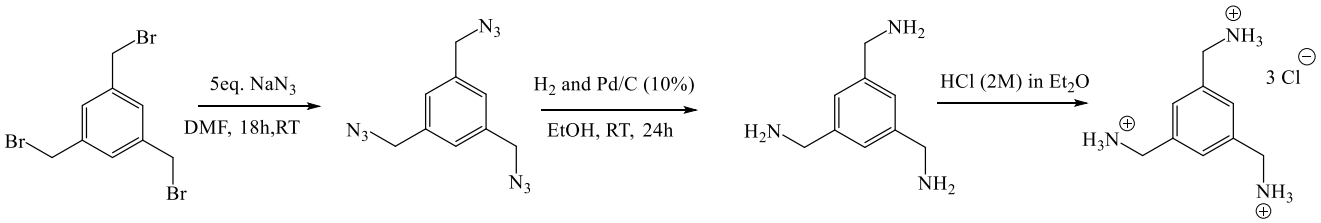

Scheme S 1: Synthesis of 1,3,5-tris(ammoniumchloridemethyl)benzene.

Synthesis of 1,3,5-tris(azidomethyl)benzene (Scheme S1): 1.58 g (4.42 mmol) 1,3,5-tris(brommethyl)-benzene and 5 equiv. 1.44 g (22.1 mmol) NaN_3 were stirred in 15 mL DMF, for 66 h at RT, while a white precipitate formed.[2] Reaction progress was monitored by TLC (SiO_2: eluent: hexane/ethyl acetate, 6:4). The precipitate was filtrated, and the filtrate was distilled to yield a white powder. The product was dissolved in 30 mL CH_2Cl_2 and extracted three times with 100 mL H_2O. The combined organic layers were dried over anhydrous $MgSO_4$. The product was filtrated, evaporated and dried to yield 521 mg (53%) of 1,3,5-tris(azidomethyl)benzene as a pale-yellow oil.

^{1}H NMR (300 MHz, $CDCl_3$): δ 7.19 (s, 3H (2.89), Ar-H), 4.27 (s, 6H (6.02), Ar-CH_2); ^{13}C{^{1}H} NMR (MHz, $CDCl_3$): δ 136.45 (s, 3C, 1,3,5-Ar-C), 126.75 (s, 3C, 2,4,6-Ar-C), 53.51 (s, 3C, CH_2); TOF MS ESI$^+$: m/z = [M$^+$] = 243.13; [M+H]$^+$= 244.12; [M+4H]$^+$ = 247.09.

Synthesis of 1,3,5-tris(ammoniumchloridemethyl)benzene (Scheme S1): 647.2 mg (2.661 mmol) 1,3,5-tris(azidomethyl)benzene were dissolved in 20 mL EtOH and stirred at RT for 24 h under hydrogen atmosphere (1 bar) in the presence of 29 mg (0.27 mmol, 10%) Pd/C.[3] The mixture was filtrated, and the filtrate was evaporated to 3–5 mL and precipitated with 20 mL HCl (2M) in diethyl ether for better handling and analysis in its ammonium chloride powder form. The white precipitate was collected by vacuum filtration and dried to give 651 mg (89%) 1,3,5-tris(ammoniumchloridemethyl)benzene.

^{1}H NMR (300 MHz, $CDCl_3$): δ 7.52 (s, 3 H (3.00), Ar-H), 4.91 (s, 6 H (6.33), Ar-CH_2), 4.10 (s, broad, 12H (5.91), NH_3Cl, the ammonium chloride is only roughly seen in the proton spectrum, and integration is less than expected. ^{13}C{^{1}H} NMR (MHz, CD_2Cl_2): δ 142.86 (s, 3C, 1,3,5-Ar-C), 134.73 (s, 3C, 2,4,6-Ar-C), 49.0 (s, 3C, CH_2). TOF MS ESI$^+$: m/z = [M$^+$] = 274.13.

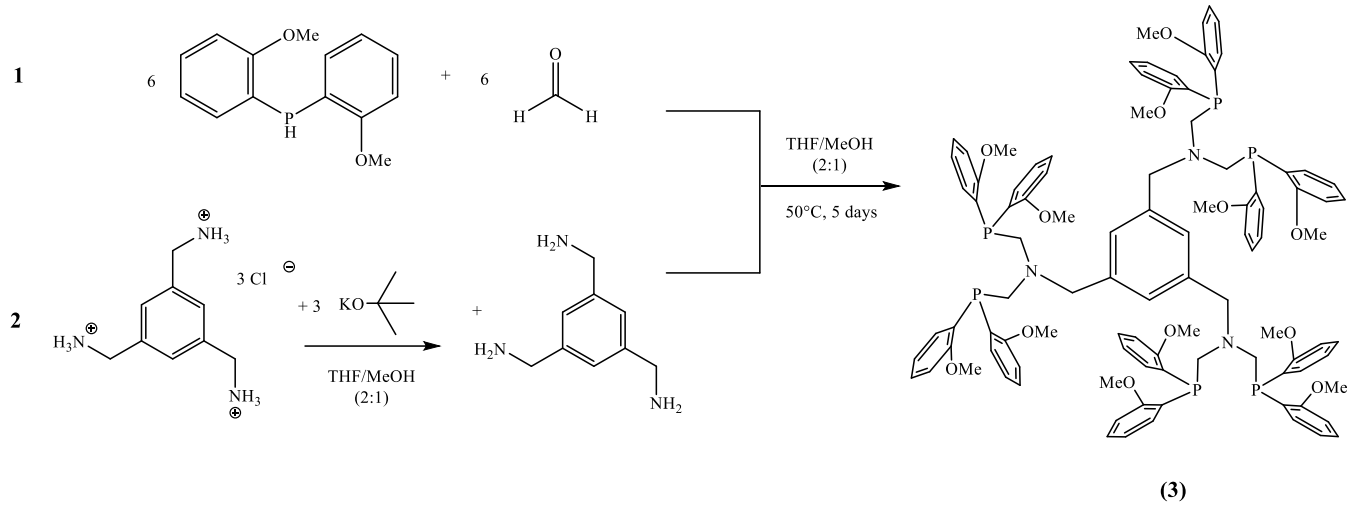

Scheme S 2: Synthetic route to 1,3,5-tris(PNP-Me)benzene (**3**).

Synthesis of 1,3,5-tris(PNP-Me)benzene (3), (Scheme S2)**:** 227.0 mg (0.96 mmol) of 1,3,5-tris(ammoniumchloridemethyl)benzene were deprotonated with 322.0 mg (2.87 mmol) potassium *tert*-butoxide in 30.0 mL of deoxygenated THF/MeOH (2:1; v/v) (mixture 2 in Scheme S2). Afterwards, 172.0 mg (5.74 mmol) paraformaldehyde and 1.41 g (5.74 mmol) bis(2-methoxyphenyl)phosphine (mixture 1 in Scheme S2) were added and stirred at 50°C for 5 days. The solvent was removed under reduced pressure. The residue was washed three times with MeOH and dried under vacuum to yield 1.23 g (75%) as a white powder.

$^{31}P\{^{1}H\}$ NMR (121.497 MHz, MeCN-d_3): δ(ppm) = -43.36 (s, 6P); ^{1}H NMR (300 MHz, MeCN-d_3): δ(ppm) = 7.28 – 6.54 (m, ($^{3}J_{HH}$ = 9.0, 12H); 7.01 – 6.95 (m, $^{3}J_{HH}$ = 9.0, 12H); 6.86 – 6.82 (dd, $^{3}J_{HH}$ = 3.0, 12H), 6.72 – 6.67 (t, $^{3}J_{HH}$ = 9.0, 12H), 6.54 (s, 3H, benzene-H)), in total 51H (51), Ar-H), 3.67 (s, 6H (6.07), Ar-CH_2-N), 3.61 (s, 36H (36.24), O-CH_3), 3.37 – 3.36 (m, $^{3}J_{HH}$ = 3.0, 12H (11.86), N-CH_2-P);

TOF MS ESI^+: m/z = 1717.81 $[M+3H]^+$;

mp: 99.4°C

3: calc. for $C_{99}H_{105}N_3O_{12}P_6$ (1714.79): C, 69.34; H, 6.17; N, 2.45. Found: C, 69.31; H, 6.19; N, 2.43%.

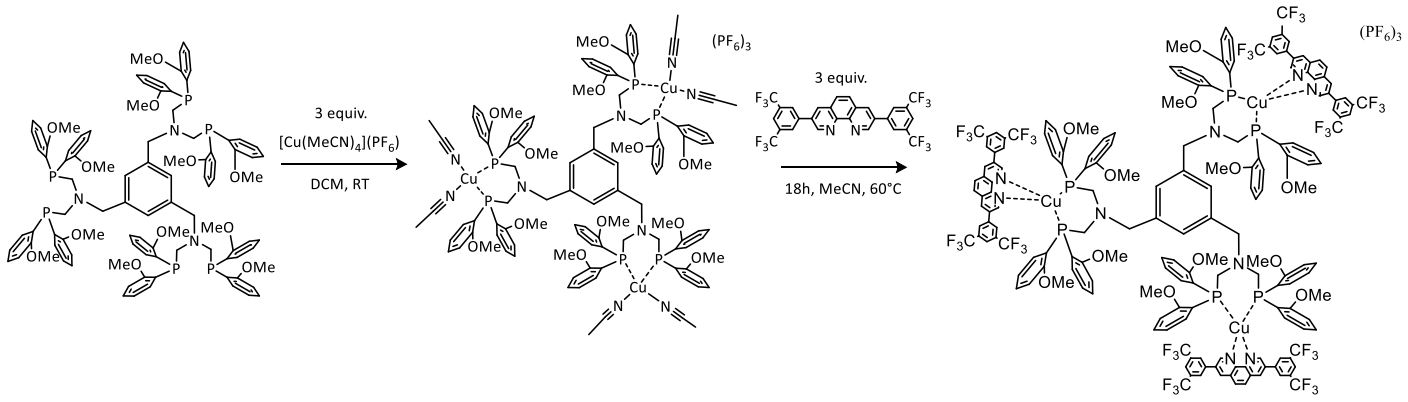

(3) **(4')** **(4d)**

Scheme S 3: Synthetic route to the complexes **4'** and **4d**.

Synthesis of [(Cu(phenanthrolinederivate))$_3$(1,3,5-tris(PNP-Me)benzene](PF$_6$)$_3$ (**4d**, Scheme S3)**:** 1.0 equiv. of **3** and 3.0 equiv. [(Cu(MeCN)$_4$](PF$_6$) or CuCl were stirred at 60°C in 30.0 mL MeCN with 3.0 equiv. 3,8-bis(3,5-bis(trifluoromethyl)phenyl)-1,10-phenanthroline for 18h. The product was precipitated with Et_2O, washed with Et_2O and dried under vacuum. The product was obtained in 84% yield as a red powder (**4d**). The solvato-complex **4'** can be isolated if the reaction is performed stepwise and not in a one-pot reaction.

4': $^{31}P\{^1H\}$ NMR (121.49 MHz, CD_2Cl_2): δ -35.3 (s, 6 P, P_2-Cu-N_2); -126.4 – -161.59 (sept, 3P, PF_6). ^1H NMR (300 MHz, CD_2Cl_2): δ 7.52 – 6.78 (m (J_{HH} = 9.0; 15.0; 6.0 Hz), 51 H (51.0), Ar-H P-ligand), 3.68 (m, 36 H (35.9), O-CH_3, 3.26 (s, 6 H (5.74), bs, Ar-CH_2-N), 3.00 – 2.97 (m, (J_{HH} = 9.0 Hz), 12 H (12.0), N-CH_2-P), 2.10 (s, 18H (18.1), ACN-CH_3)

4d: $^{31}P\{^1H\}$ NMR (121.49 MHz, $CDCl_3$/THF-d_8): δ -24.6 (s, 6 P, P_2-Cu-N_2); -132.1 – -155.6 (sept, 3 P, PF_6).^1H NMR (300 MHz, $CDCl_3$/THF-d_8): δ 8.59– 7.62 (s, d, d (J_{HH} = 9.0; 15.0 Hz), Ar-H phenanthroline-derivate), 7.28 – 6.02 (m (J_{HH} = 6.0; 9.0; 9.0; 6.0 Hz) Ar- P-ligand),in total 87H (36H+51H); 3.48 (s, 12 H (11.64), P-CH_2-N); 3.12 (s, 36 H (36.64), O-CH_3), , 2.31 -2.28 (d, (J_{HH} = 9.0 Hz) 6 H (6.59); N-CH_2-benzene).

TOF MS ESI$^+$: m/z = 668.91 [fluorophen-Cu(I)$^+$+ H$^+$]; 667.89 [fluorophen-Cu(I)$^+$]; 666.95 [fluorophen-Cu(I)$^+$ - H$^+$]; 605.91 [3,8-bis(3,5-bis(trifluoromethyl)phenyl)-1,10-phenanthroline + H$^+$]; 956.09 [$C_{44}H_{31}CuF_{12}N_3O_2P_2^{\bullet+}$]; 1288.52 [$C_{65}H_{49}CuF_{12}N_3O_4P_2^{2\bullet+}$].

The compound is fragmented strongly when measured with ESI-MS. MALDI-TOF-MS was not suitable. However, it was possible to fully characterise **4d** in its BF_4^- form by a single crystal X-ray structure analysis (*vide infra*).

mp: >300°C (dec). **4d**: calc. for $C_{188.52}H_{156.33}B_3Cu_3F_{48}N_{9.86}O_{14.95}P_6$ (4119.95): C, 54.96; H, 3.82; N, 3.35. Found: C, 54.91; H, 3.85; N, 3.32%.

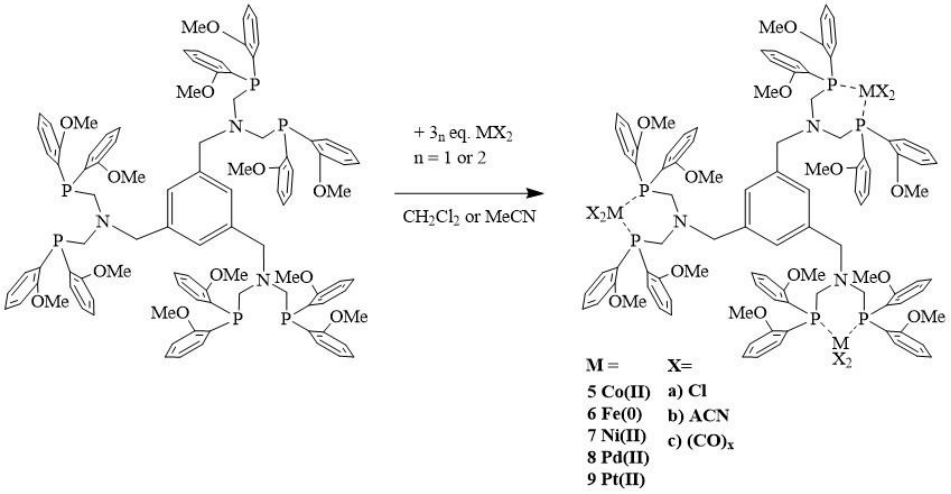

Scheme S 4: Synthetic route to complexes **5**–**9**.

Synthesis of [($CoCl_2$)$_3$tris(PNP-Me)benzene] (5a): 20.0 mg (11.7 µmol) of 1,3,5-tris(PNP-Me)benzene and 3.0 equiv. (35.0 µmol) $CoCl_2 \cdot 6\ H_2O$ were dissolved in 10.0 mL CH_2Cl_2 and stirred at RT for 19 h. The turquoise solution was filtrated, the solvent removed under reduced pressure and precipitated with hexane to obtain 11.3 mg (46%) of a green-black powder.

$^{31}P\{^1H\}$ NMR (121.49 MHz, CD_2Cl_2): paramagnetic, negative control: no uncoordinated ligand visible at δ - 46 ppm.

ESI-MS m/z = 2156.21 $[M + 3\ H_2O - 2H]^+$. mp: >300°C (dec). **5a**: calc. for $C_{99}H_{105}Cl_6N_3O_{12}P_6Co_3$ (2104.29): C, 56.51; H, 5.03; N, 2.00. Found: C, 56.48; H, 5.07; N, 1.98%.

Synthesis of [($Fe_3(CO)_9$(μ,η^2-CO)$_2$)$_3$(μ,η^2-1,3,5-tris(PNP-Me)benzene)] (6c): 40.1 mg (23.4 µmol) 1,3,5-tris(PNP-Me)benzene were added to a solution of 6.0 equiv. $[Fe_3(CO)_{12}]$ in ACN and refluxed at 80°C for 4 h. Afterwards the red solution was cooled down to RT and stirred for additional 16 h. The mixture was filtrated and evaporated to yield 26.7 mg (74%) as a red-brown powder.

$^{31}P\{^1H\}$ NMR (121.49 MHz, ACN): δ 39.97 (s, 6 P, P_2- $[Fe_3(CO)_9(\mu,\eta^2\text{-}CO)_2(\mu, \eta^2P_2R)]$; ^1H NMR (300 MHz, MeCN-d_3): δ 7.50 – 7.02 (broad overlapping peaks, 51H (51), Ar-H), 3.78 – 3.63 (broad overlapping peaks of O-CH_3, Ar-CH_2-N and N-CH_2-P in total 54H (53.4))**.** All obtained NMR data of **6c** show very broad signals, which could be due to partially high spin properties. These data were compared to the reported data from E. Stein and F. Y.Fujiwara.[4]

IR spectroscopy: iron carbonyls: ν cm^{-1}: endo C-O stretch: 2042 (s); 1993 (νs); terminal carbonyls: 1965 (vs); 1932 (vs)**;** bridging carbonyls: 1731(w); 1672 (w); ν_{as} (C=O): 1589 (s); 1575 (s); 1477 (s); 1463(s); 1431.8 (s); ν(C-O): 1276(s); 1247 (s); 1201 (s); Ligand: P-C stretch: 625 (νs); P-Ar stretch: 1164-1021 (s), ν (OCH_3) = 1021 (s). *The collected ^{31}P NMR and IR data were in accordance with the reported data for bidentate phosphine iron carbonyl complexes.*[4] ESI-MS m/z = 3142.75 $[M + H]^+$. mp: >300°C (dec). **6c**: calc. for $C_{132}H_{105}N_3O_{45}P_6Fe_9$ (3141.74): C, 50.46; H, 3.37; N, 1.34. Found: C, 50.42; H, 3.40; N, 1.30%.

Synthesis of [($NiCl_2$)$_3$(1,3,5-tris(PNP-Me)benzene)] (7a): 30.0 mg (17.5 µmol) 1,3,5-tris(PNP-Me)benzene and 3.0 equiv. (52.5 µmol) nickel(II) chloride ethylene glycol dimethyl ether complex were stirred in CH_2Cl_2 at 30°C for 18 h. The red filtrate was precipitated with hexane to yield 20.0 mg (79%) as a red powder.

$^{31}P\{^1H\}$ NMR (121.49 MHz, CD_2Cl_2): δ 3.27 (bs, 6 P, P_2-$NiCl_2$)

^1H NMR (300 MHz, MeCN-D_3/$CDCl_3$): δ 7.51– 6.00 (s (3.64H), m (18.11H, J_{HH} = 6.0 Hz), m (26.19H, J_{HH} = 3.0 Hz), s (3.06H) in total 51 H (51.08), Ar-H), 3.59 – 3.57 (m, 36 H (O-CH_3) + 12 H (N-CH_2-P) (in total 48 H), 3.00 (s, 6 H (6.02), Ar-CH_2-N)**.**

ESI-MS *m/z* = 2068.12 $[M - Cl]^+$.

mp: >300°C (dec). **7a**: calc. for $C_{99}H_{105}Cl_6N_3O_{12}P_6Ni_3$ (2103.57): C, 56.53; H, 5.03; N, 2.00. Found: C, 56.50; H, 5.05; N, 1.96%.

Synthesis of $[(Ni(ACN)_2)_3$(1,3,5-tris(PNP-Me)benzene)$](PF_6)_6$ (7b): The chlorido-complex (20.0 mg) was stirred for18 h in ACN with 24.0 equiv. $TIPF_6$, which precipitates as TlCl and can be removed by filtration. The orange red filtrate was evaporated resulting in **7b** (28.0 mg, 98% yield, red-orange powder).

$^{31}P\{^1H\}$ NMR (121.49 MHz, MeCN): δ -11.91 (bs, 6 P, P_2-$NiACN_2$), -125.643 – -160.746 (sept, PF_6);

^1H NMR (300 MHz, MeN-d_3): δ 7.49– 6.64 (t, d, s, m, (J_{HH} = 6.0; 6.0; 9.0 Hz), 51 H (51), Ar-H), 4.03 (s, 36 H (36.29), O-CH_3), 3.59; 3.30 (s, s, 6 H (4.22 + 1.74)), Ar-CH_2-N), 3.48 (s, 12 H (12.24), N-CH_2-P), 1.94 (s, MeCN-CH_3 overlapping with solvent signal).

ESI-MS m/z = 2524.57 $[M - 3PF_6 – MeCN - 6H]^+$.

mp: >300°C (dec). **7b**: calc. for $C_{111}H_{123}F_{36}N_9O_{12}P_{12}Ni_3$ (3006.96): C, 44.34; H, 4.12; N, 4.19. Found: C, 44.31; H, 4.15; N, 4.16%.

Synthesis of $[(PdCl_2)_3$(1,3,5-tris(PNP-Me)benzene)] (8a): 39.4 mg (22.9 µmol) 1,3,5-tris(PNP-Me)benzene and 3.0 equiv. $PdCl_2$(COD) (68.7 µmol) were dissolved in 15.0 mL CH_2Cl_2 and stirred at RT for 18 h. The crude product was precipitated with hexane and washed with MeOH to obtain a yellow powder (24.4 mg, 62%).

$^{31}P\{^1H\}$ NMR (121.49 MHz, MeCN-d_3): δ 7.66 (s, 6 P, P-$PdCl_2$).

^1H NMR (300 MHz, MeCN-D_3): δ 7.91 – 6.05 (m, m, m, s (J_{HH}= 6.08; 3.0; 9.0 Hz), 51 H (14+36+1 in total 51H), Ar-H), 3.93 (bs, 36 H (36.1),), 3.63 – 3.43 (m, (J_{HH}= 3.0 Hz), 54 H (6+12+36), overlapping peaks of O-CH_3, Ar-CH_2-N and N-CH_2-P).

ESI-MS m/z = 2211.30 $[M - Cl]^+$.

mp: >300°C (dec). **8a**: calc. for $C_{99}H_{105}Cl_6N_3O_{12}P_6Pd_3$ (2246.75): C, 52.92; H, 4.71; N, 1.87. Found: C, 52.88; H, 4.74; N, 1.86%.

Synthesis of $[(Pd(ACN)_2)_3$(1,3,5-tris(PNP-Me)benzene)$](PF_6)_6$ (8b): To 24.4 mg **8a**, 10.0 equiv. $TIPF_6$ were added and stirred in MeCN for 47 h, while a white TlCl precipitate was formed, which was removed by filtration. The yellow filtrate was evaporated and washed three times with degassed H_2O, filtrated and dried to yield 20.5 mg (60%) as a yellow powder.

$^{31}P\{^1H\}$ NMR (121.49 MHz, MeCN-d_3): δ -5.90 (s, 6 P, P-$Pd(ACN)_2$), -120.35 – -160.74 (m, 6 P, PF_6)**;**

^1H NMR (300 MHz, MeCN-d_3): δ 7.93 – 6.75 (m, m, m, m (J_{HH} = 6.9; 1.8; 8.4; 5.7 Hz), 51 H (51), Ar-H), 4.07, 3.93, 3.75 (bs, all overlapping O-CH_3, Ar-CH_2-N and N-CH_2-P 54H (6+12+36) (53.98), 1.96 – 1.93 (m, (J_{HH}= 2.4 Hz), 18 H overlapping with solvent signal, MeCN-CH_3).

ESI-MS m/z = 2572.30 $[M - 3PF_6 – MeCN - 6H]^+$.

mp: >300°C (dec). **8b**: calc. for $C_{111}H_{123}F_{36}N_9O_{12}P_{12}Pd_3$ (3150.14): C, 42.32; H, 3.94; N, 4.00. Found: C, 42.31; H, 3.97; N, 3.98%.

Synthesis of [($PtCl_2$)$_3$(1,3,5-tris(PNP-Me)benzene)] (9a): 17.1 mg (0.01 mmol) 1,3,5-tris(PNP-Me)benzene and 3.0 equiv. (9.9 mg, 0.03 mmol) $PtCl_2$(COD) were stirred at RT in 15.0 mL ACN. The red solution bleached overnight. Reaction progress was monitored by ^{31}P NMR. The crude product was precipitated with diethylether and washed with MeOH to obtain a yellow powder (10.8 mg, 43%).

$^{31}P\{^1H\}$-NMR (121.49 MHz, MeCN-d_3): δ -8.95 (s, 6P, P-$PtCl_2$, J_{PPt} = 3565.9 Hz); 6.507; -22.846 (satellites, P-Pt, J_{PPt}= 3565.93 Hz)

^{1}H NMR (300 MHz, CD_2Cl_2): = 7.93 – 6.07 (3m (J_{HH}= 9.0; 6.0; 3.0 Hz), 51 H (51), Ar-H), 3.65 (s, 6 H (6.25), Ar-CH_2-N), 3.42 (s, 36 H (36.07), O-CH_3) 3.07 (s, 12 H (11.66), N-CH_2-P);

$^{195}Pt\{^1H\}$-NMR (64.22 MHz, CD_2Cl_2): δ -4549.57

ESI-MS m/z = 2477.28 $[M - Cl]^+$.

mp: >300°C (dec). **9a**: calc. for $C_{99}H_{105}Cl_6N_3O_{12}P_6Pt_3$ (2512.73): C, 47.32; H, 4.21; N, 1.67. Found: C, 47.29; H, 4.23; N, 1.66%.

Synthesis of [($Pt(ACN)_2$)$_3$(1,3,5-tris(PNP-Me)benzene)](PF_6)$_6$ (9b): 10 equiv. (38.4 mg; 0.11 mmol) $TlPF_6$ were added to a mixture of **9a** (28.4 mg, 0.011 mmol) in ACN and stirred for 16 h. TlCl precipitates as white suspension, which was removed by filtration. The crude product was precipitated with diethyl ether to give 5.3 mg (14%) as a yellow powder.

$^{31}P\{^1H\}$ NMR (121.49 MHz, MeCN): δ -8.24 (s, 6 P, P-$Pt(ACN)_2$, J_{PPt} = 3357.45 Hz), -160 – -125 (sept, 6 P, PF_6).

^{1}H NMR (300 MHz, dmso-d_6): = 7.51 – 6.08 (3m (J_{HH}= 6.0; 3.0 Hz), 51 H (51), Ar-H), 3.61 (s, 12 H (12), P-CH_2-N), 3.41 (s, 36 H (36.46), O-CH_3), 3.07 (s, 6 H (6.38), Ar-CH_2-N), 2.09 (s, 18 H (6, 12 H are hidden by dmso), ACN-CH_3).

ESI-MS m/z = 2660.96 $[M - 3PF_6 – MeCN - 6H]^+$.

mp: >300°C (dec). **9b**: calc. for $C_{111}H_{123}F_{36}N_9O_{12}P_{12}Pt_3$ (3416.12): C, 39.03; H, 3.63; N, 3.69. Found: C, 39.01; H, 3.64; N, 3.66%.

2. Instrumental and methods

2.1. UV/Vis and photophysical measurements :

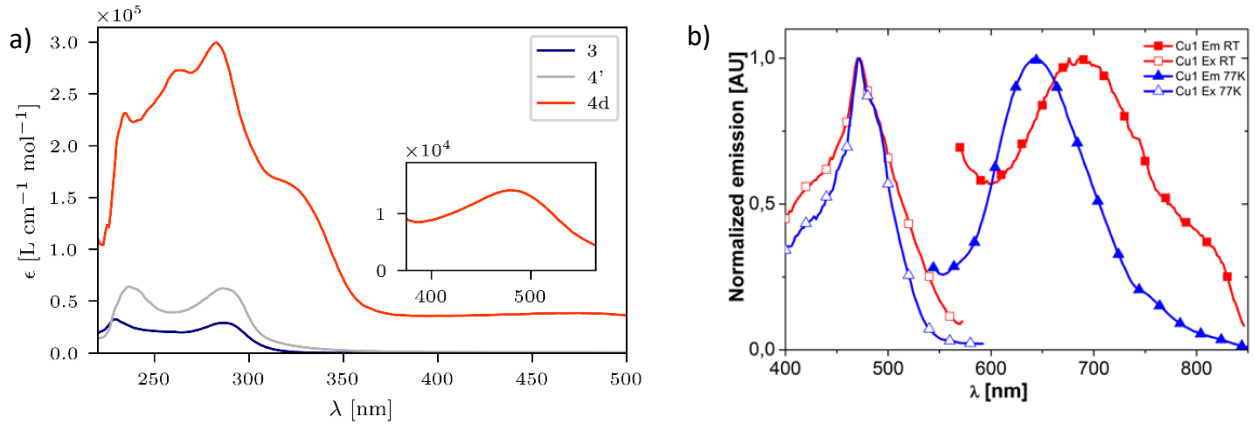

Figure S 1: a) UV-vis absorption spectra of the 1,3,5-ligand **3**, solvato complex **4'** and chromophore **4d** captured in dry MeCN. **4d** exhibits an absorption maximum at 283 nm. Insert: zoomed in region of the MLCTs of **4d** with an absorption maximum of 480 nm. b) Excitation (for emission at 688 nm, R.T., and 630 nm at 77 K) and emission spectra of **4d** (for excitation at 470 nm) in MeCN at RT and in methyl-THF at 77K.

Table TS 1: Optical and photophysical data of **4d**. Captured in MeCN at RT and in methyl-THF at 77K.

$\lambda_{max,\ RT}$ (nm)	Φ_{RT}	τ_{RT} (ns)	$k_{r,\ RT}$ (s^{-1})	$k_{nr,\ RT}$ (s^{-1})	$\lambda_{max,\ 77K}$ (nm)	τ_{77K} (ns)	A_{max} (nm)	A_{MLCT} (nm)
688	0.001	5.8	1.7×10^5	1.7×10^8	645	5.5	283	480

2.2. Cyclic voltammetry

All measurements were captured in dry MeCN with a glassy carbon working electrode and $Ag/AgNO_3$ reference electrode and a platinum counter electrode. After the measurement ferrocene was added as a reference. The cyclic voltammogram of the ligand **3** (Figure S2a) and of the compound **7a** (Figure S2b) with a defined amount of water is depicted. Upon addition of water again catalytic hydrogen release waves are observable.

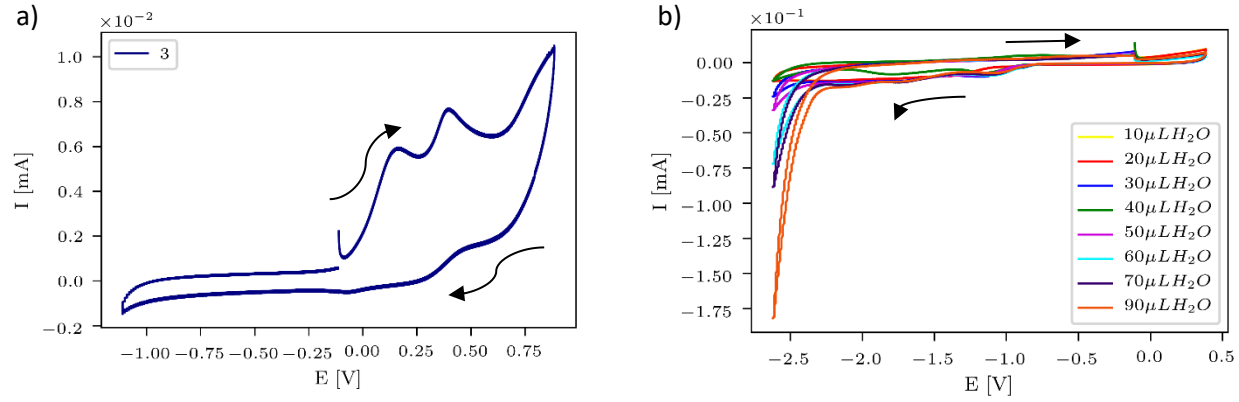

Figure S 2: Cyclic voltammogram of a) of the ligand **3** (blue) and b) of **7a** with a defined amount of water. *Solvent: dry MeCN, electrodes: WE: glassy carbon GC, RE: $Ag/AgNO_3$, CE: Pt. E is measured vs. Fc/Fc+.*

3. Irradiation experiments

3.1. Set up and experimental details

All irradiation experiments were performed in a closed Schlenk flask system with a defined amount of solvent mixture with triethylamine as a sacrificial donor (Table TS2). For the chromophore **4d** two different lamps (Table TS3, entries 1 and 2) were tested in combination with the literature known WRCs **1**, [Ni(py-S)$_3$] and **2**, [Fe$_3$(CO)$_{12}$] to optimise the final TON of the chromophore.

For the WRCs **5–9** the two irradiation sources (Table TS3, entries 2 and 3) were tested and compared in terms of their activity, and endurance.

The volumes of the irradiations and the related Schlenk systems are defined in Table TS4. References (manuscript, Tables 3 and 4) were measured without the new complexes to ensure the dependence of the hydrogen production on the compounds.

Table TS 2: Used irradiation solutions.

entry	Irradiation solution (v:v:v)	pH
1	200 mL MeCN, 50 mL TEA, filled up to 500 mL in a round flask with H_2O	10.00 adjusted with HCl (1M)
2	THF/TEA/H_2O (3.2:1)	10.27
3	THF/TEA/H_2O (4.3:1)	10.55

Table TS 3: Irradiation sources for the irradiation experiments.

entry	Irradiation. source	spectrum	intensity	annotations
1	LED-tower	405 nm 447 nm 525 nm	6 x 250mW 6 x 280mW 6 x 550mW	focused beam, defined wavelength
2	700W Hg medium pressure lamp	250 – 450nm, 550 – 600nm	700W	broad distribution, broad spectrum
3	LED- Solar Light Lab Luminaire*	UV, 470nm, 515nm, cold white	0 – 200W	focused beam, wavelength and intensity adjustable

Table TS 4: Irradiation flasks used for the irradiation experiments.

entry	Schlenk type	V (mL range)
A	quartz Schlenk: permeable for UV light: 200 – 280 nm	V = 15 – 25 mL
B	standard glass Schlenk: permeable >280 nm	V = 20 – 365 mL

3.2. Control experiment: Irradiation with D_2O and D_2 measurement

The irradiation of the best performing WRC **8b** tris(Pd(ACN)$_2$)$_3$ in deuterated H_2O provides information about the catalytic cycle and kinetic effects. The produced hydrogen is presumed to be generated from water. An experiment in D_2O allows the determination of the produced D_2 from D_2O. Since the analysis by GC is sensitive to both D_2 and H_2 an additional measurement with a calibrated sector field mass spectrometer (HSense) was examined. The irradiation experiment was performed under the same conditions as the experiment with water (Figure S 3, blue) but with D_2O instead of H_2O. The measured hydrogen via GC and the D_2 via HSense from the same experiment were compared (Figure S 3, red and dark blue). The comparison of the experiment with water showed almost a double TON value (blue). Since deuterium is twice as heavy as a proton, the catalytic process is influenced by the kinetic isotope effect [5]. Therefore, the formation or cleavage of X-D bonds need more activation energy than for X-H bonds and result in slower reactions.[5,6] Additionally, the transport mechanism and diffusion coefficient is slower and smaller in the case of D_2O.[7] Thus, indicating a smaller TON for the D_2O experiment. Furthermore, this experiment demonstrated that the protons were provided from water. Another deviation is the pH value for the solution with D_2O, which differs slightly. The pH value in this experiment of the D_2O is 11.925, and from the H_2O solution is 11.066.

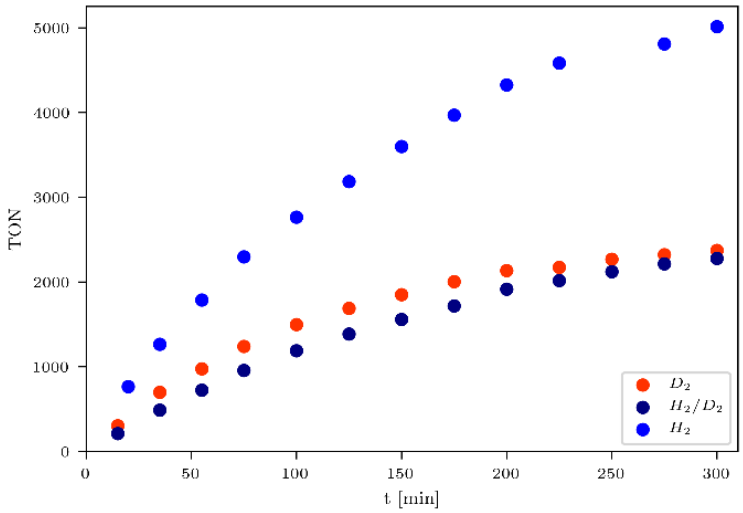

Figure S 3: Kinetic isotopic effect: D_2 measurement with a sector field mass spectrometer (HSense) in comparison to H_2. The experiment was conducted with the catalyst **8b** (0.32 µmol) and 6 eq. [Ir(bpy)(ppy)$_2$](PF$_6$) chromophore in 15 mL solvent (THF/TEA/H_2O or D_2O (3:2:1)). Blue: H_2 via GC; red: D_2 via MS; dark blue: indistinguishable H_2/D_2 via GC, indicating that irradiation of the D_2O solution solely delivers D_2 and no H/D exchange with THF or TEA occurs.

3.3. Incident photon conversion efficiency (IPCE):

The used irradiation source "Solar Light Lab Luminaire" (Figure S 4) was developed by the Bartenbach Holding GmbH. More information can be found in "Lichtreaktor sowie Verfahren zur synthetischen Stofferzeugung mittels Lichtbestrahlung. Patent pending, 202012111705220ODE, 2020."

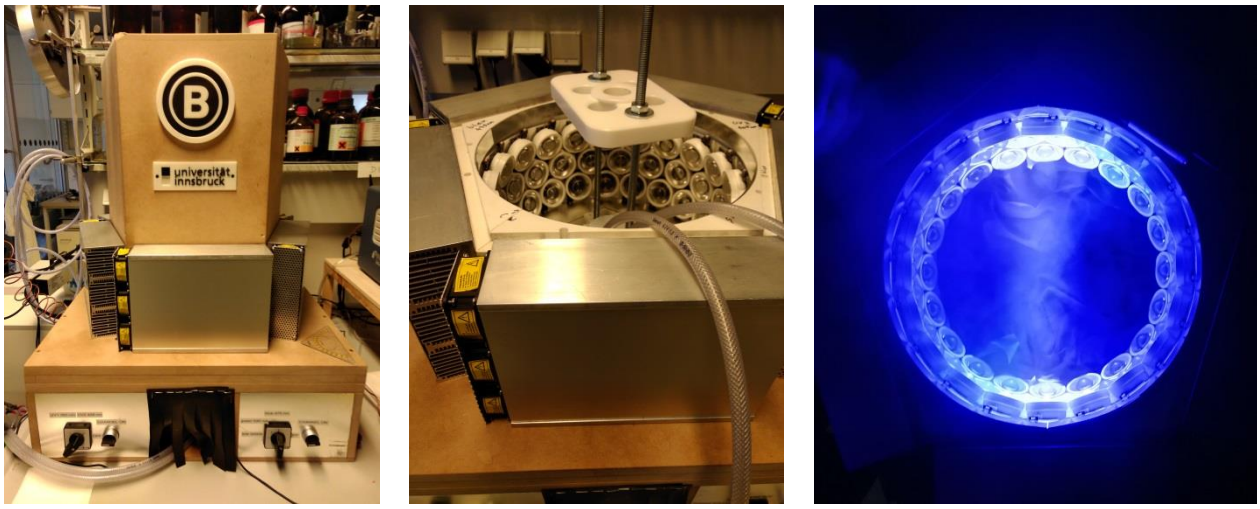

Figure S 4: Photoreactor (left) with the irradiation chamber (middle) and its irradiation geometry shown with 470 nm light (right).

3.4. Irradiation Experiments with the Newly Developed Bartenbach Photoreactor.

In order to make the calculation of the incident photon conversion efficiency (IPCE) as given in the article possible, the following calibration has been performed (Pann J., PhD thesis, University of Innsbruck, 2022). To investigate the reproducibility and the capabilities of the photochemical reactor, experiments with a chemical actinometer, initially proposed by Hatchard and Parker in 1956, [8,9] were performed, and compared with the measurements of the integrated semiconductor based photometer.

For consistency, the unit of the amount of photons per surface and time interval is chosen to be photon fluence ($m^{-2}s^{-2}$, or $Em^{-2}s^{-1}$), according to the IUPAC Gold Book.[10] For comparability with literature and measurement devices the value of the photon fluence is also given in $Emin^{-1}cm^{-1}$, $s^{-1}nm^{-2}$ for multiphoton absorption processes and kWm^{-2} for instrumental reasons.

The "ferrioxalate-" or "Hatchard and Parker actinometer" consists of an acidified $K_3Fe(C_2O_4)_3$ solution that reacts with photons in the range of 280-450 nm to produce Fe^{II} and CO_2 (eq. 1.1). The Fe^{II} is then photometrically determined by the absorption of $[Fe(phen)_3]^{2+}$ at 510 nm (ε = 11100 $Lmol^{-1}cm^{-1}$).

1.1 $$2\,K_3Fe(C_2O_4)_3 + h\nu \rightarrow 2\,K_2Fe(C_2O_4)_2 + 2\,CO_2 + K_2C_2O_4$$

The quantum efficiency of this reaction is tabulated in the literature, and is 0.56 (5) for 405 nm and 0.50(2) for 436 nm as well as not influenced by the temperature between 5 °C and 80 °C.[11] Grüter and Demas showed the applicability of the ferrioxalate actinometer at high photon flux densities in laser light setups. The actinometer shows linear responsiveness to the number of incident photons at photon fluence of $2.8 * 10^{-4}$ $Emin^{-1}cm^{-1}$ or $2.8*10^4$ $s^{-1}nm^{-2}$ or 6.2 kWm^{-2}.[12,13]

For small wavelengths (<420 nm) and low light intensities (<0.3 kWm^{-2}) an irradiation solution of 0.0067 M $K_2Fe(C_2O_4)_3$ in 0.05 M H_2SO_4 and for higher intensities and wavelengths up to 470 nm a 0.15 M $K_2Fe(C_2O_4)_3$ in 0.05 M

H_2SO_4 was used. After irradiation, an aliquot (0.1 to 0.00067) was treated with a sodium acetate buffered phenanthroline (0.1 % 1,10-phenanthroline, 1.65 M NaOAc, 0.5M H_2SO_4) solution to obtain a reasonably diluted $[Fe(phen)_3]^{2+}$ solution suitable for photometry.

The handling of the solutions was performed under red or very low light levels. The photoreactor was set to a certain light power via the integrated photometer ("1–200 mW"). After an equilibration time of 15 minutes 15.0 mL of the $K_2Fe(C_2O_4)_3$-solution was equipped with a stirring bar placed in an 30 mm irradiation Schlenk flask. The solution was stirred and irradiated for the desired amount of time (10–200 s). After the irradiation, the 0.15 M solution was diluted (1:50) with water and in turn diluted (3:10) with the buffered phenanthroline solution. The 0.0067 M $K_2Fe(C_2O_4)_3$-solution was diluted (1:10) with the buffered phenanthroline solution. The resulting red solution's absorbance was measured with respect to a non-irradiated, but equally treated reference sample.

3.5. Data analysis

From the absorbance, the quantum yield, the absorption coefficient and dilution factor, the incident photon number was calculated with the following formulae (eq. 1.2 and 1.3):

1.2
$$N_p = \frac{Abs - Abs_{Ref}}{11100 * 2} * \frac{1}{\Phi_{\lambda,1}} * \frac{1}{f} * V$$

N_p	Number of photons interacted with the solution	/E
Abs	Absorbance of the irradiated and complexed Fe solution at 510 nm	
Abs_{Ref}	Absorbance of the complexed Fe reference solution at 510 nm	
f	Dilution factor	
V	Volume of the irradiated solution	/L
$\Phi_{\lambda,1}$	Quantum yield at wavelength λ (0.57 for 405 nm, 0.61 for 450 nm)	

where

1.3
$$H_{p,o} = \frac{N_p}{A_s * t}$$

N_p	Number of photons interacted with the solution	/E
A_s	Cross section of the irradiated volume	/m²
$H_{p,o}$	Photon fluence rate	/Em^{-2}s^{-1}
t	Irradiation time	/s

Table TS 5: Calculation table for the actinometric and photometric evaluation.

			Actinometer			Photodiode			
			Diluted Sol.						
$c(K_3Fe_3(C_2O_4)_3)$	t	f	Delta Abs	Incident photons	Photon fluence	Power	Wavelength	Incident photons	Photon fluence
/M	/ s			/ E	/(s*nm²)	/ mW	/nm	/ E	/(s*nm²)
0,0060	180	0,10000	1,184	1,4E-05	6,1E+01	1,0	405	1,5E-05	6,7E+01
0,0060	150	0,10000	1,056	1,3E-05	6,6E+01	1,0	405	1,3E-05	6,7E+01
0,0060	70	0,10000	0,473	5,6E-06	6,3E+01	1,0	405	6,0E-06	6,7E+01
0,0060	20	0,10000	1,368	1,6E-05	6,4E+02	10,0	405	1,7E-05	6,7E+02
0,0060	20	0,10000	1,400	1,7E-05	6,5E+02	10,0	405	1,7E-05	6,7E+02
0,0060	20	0,10000	1,452	1,7E-05	6,8E+02	10,0	405	1,7E-05	6,7E+02
0,0060	20	0,10000	1,402	1,7E-05	6,5E+02	10,0	405	1,7E-05	6,7E+02
0,1500	40	0,00667	1,059	1,9E-04	3,7E+03	50,5	405	1,7E-04	3,4E+03
0,1500	40	0,00667	1,062	1,9E-04	3,7E+03	50,5	405	1,7E-04	3,4E+03
0,1500	40	0,00667	1,866	3,3E-04	6,5E+03	100,1	405	3,4E-04	6,7E+03
0,1500	40	0,00667	2,061	3,7E-04	7,2E+03	100,1	405	3,4E-04	6,7E+03
0,1500	40	0,00667	1,910	3,4E-04	6,7E+03	100,1	405	3,4E-04	6,7E+03
0,1500	40	0,00067	0,258	4,6E-04	9,0E+03	153,5	405	5,2E-04	1,0E+04
0,1500	40	0,00067	0,273	4,9E-04	9,6E+03	153,5	405	5,2E-04	1,0E+04
0,1500	20	0,00067	0,236	4,2E-04	1,7E+04	199,0	405	3,4E-04	1,3E+04
0,1500	20	0,00067	0,213	3,8E-04	1,5E+04	199,0	405	3,4E-04	1,3E+04
0,1500	40	0,00667	0,251	4,2E-05	8,3E+02	10,3	450	3,9E-05	7,7E+02
0,1500	200	0,00667	1,113	1,9E-04	7,3E+02	10,3	450	2,0E-04	7,7E+02
0,1500	40	0,00667	2,289	3,8E-04	7,5E+03	99,8	450	3,8E-04	7,4E+03

For evaluation, the amount of photons detected by the actinometer and the photometer were plotted logarithmically against each other.

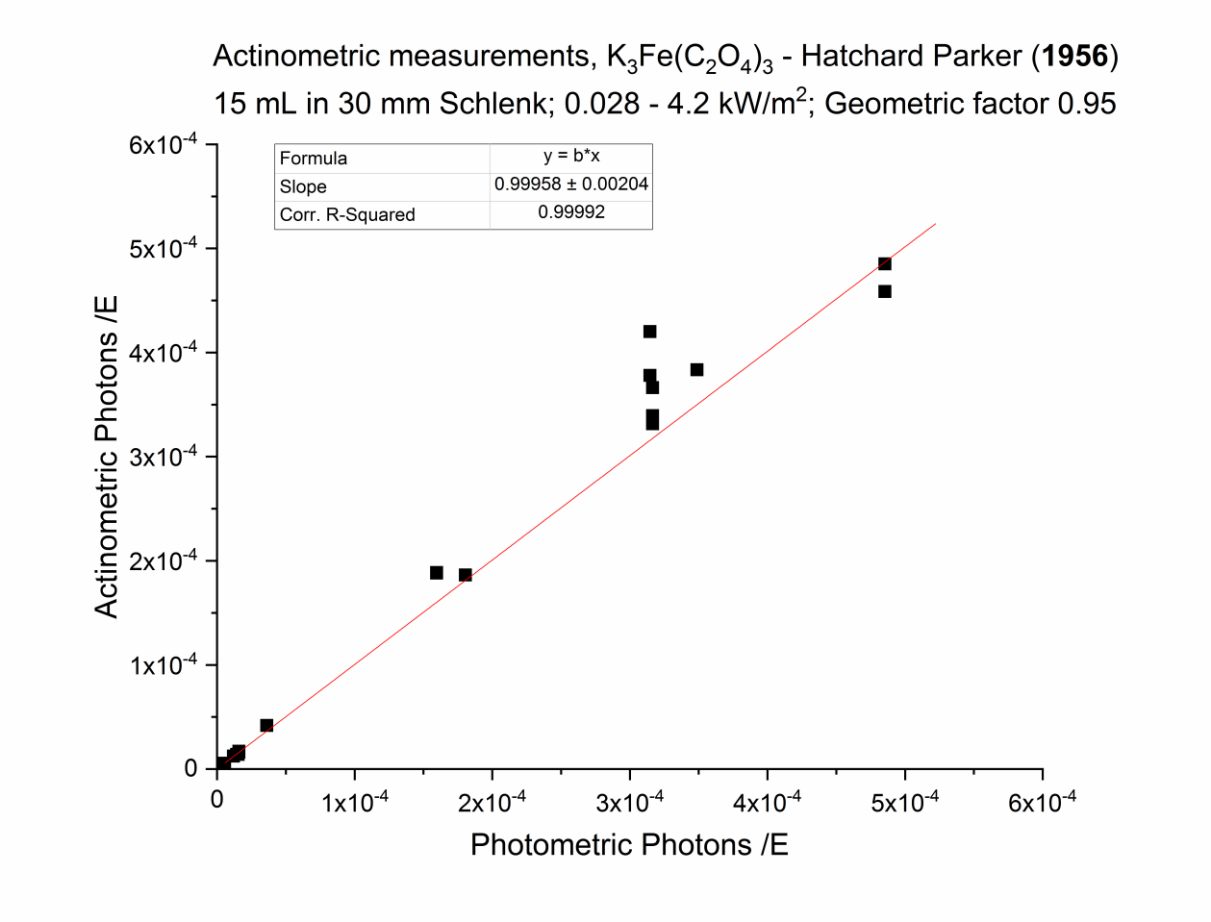

Figure S 5: Logarithmic plot of the number of photons detected via the actinometric method and via the semiconductor based photometer.

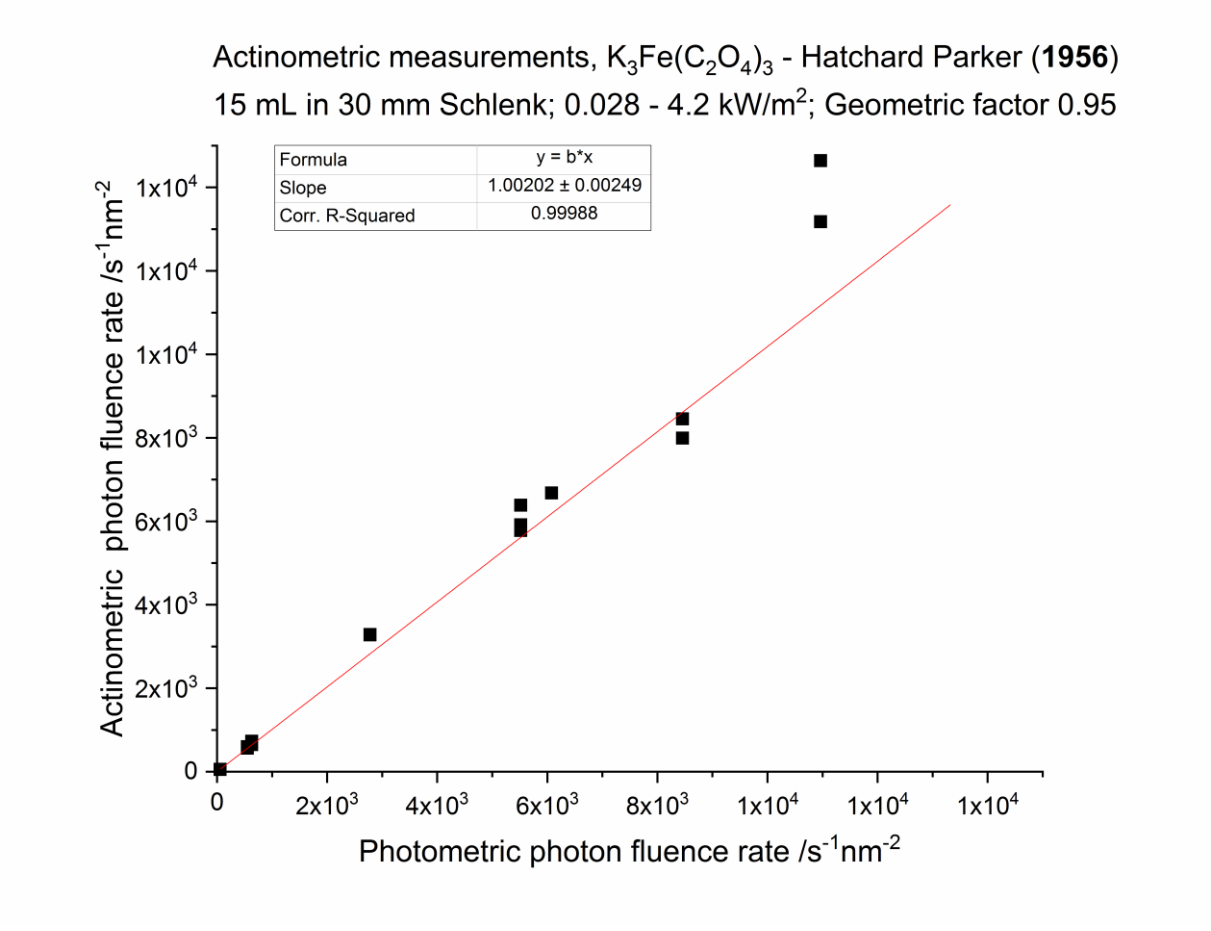

Figure S 6: Logarithmic plot of the photon fluence detected via the actinometric method and via the semiconductor based photometer.

As explained in the technical documentation of the irradiation tower, for the photon flux measurement, it is crucial to know the geometric factors of the irradiated solution. For the 30 mm Schlenk flasks filled with 15.0 mL of actinometric solution, the roughly estimated geometric factor is 0.91 from the inhomogeneity of the field, times 1.31 for the three-dimensionality of the solution. Resulting in a geometric factor of 1.19. This factor relates the photometrically measured photon flux and the actual photon flux on the solution cross section. With the actinometer the previously approximated value can be determined more exactly, to be 0.95 for this setup (0.954 and 0.949 for 405 nm and for 450 nm setup, respectively). With this geometric factor the results show an excellent linearity with respect to the number of photons irradiated on the solutions (0.992, s = 0.003, Figure S 5) as well with respect to the photon flux (1.009, s = 0.004, Figure S 6).

With the evaluation of the linearity of these descriptors, a direct determination of the incident photon count (IPC) and the resulting quantum yield (Φ_λ) of the photochemical reaction is possible via the application of the semiconductor based photometer and the geometry of the irradiated solution (eq. 1.4 and 1.5).

1.4
$$IPC = \frac{P * t * A_s * U * \lambda}{A_p * h * c * N_a}$$

P	Power of the photodiode photometer	/W
t	Irradiation time	/s
A_s	Cross section of the irradiated Solution, perpendicular to the incident light	/m²
U	Geometric factor (= 0.95)	
λ	Wavelength of the irradiation light	/m
A_p	Measuring surface of the photodiode	/m
h	Planck's constant	/Js^{-1}
c	Vacuum speed of light	/ms^{-1}
N_a	Avogadro's number	
IPC	Incident photon count	/E

1.5
$$\Phi_\lambda = \frac{N * s}{IPC}$$

Φ_λ	Quantum yield of a reaction for the wavelength of λ	
N	Number of reaction products (eg.: Mol H_2 …)	/mol
s	Stoichiometric factor	

3.6. Results

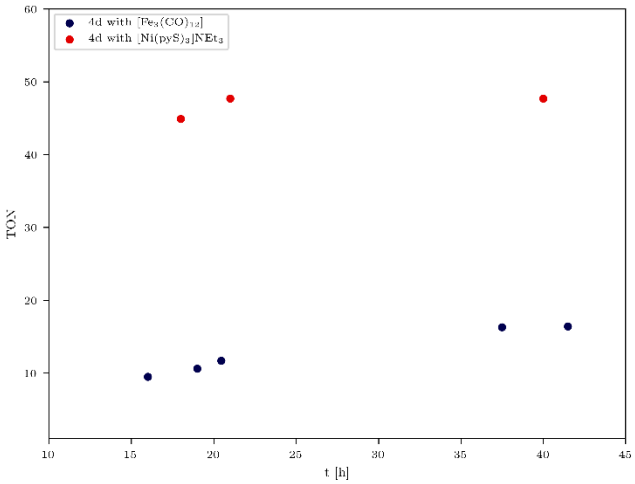

Figure S 7: TONs of **4d** with $[Fe_3(CO)_{12}]$ and 700W Hg irradiation (blue) and with $[Ni(py\text{-}S)_3](NEt_4)$ after exposure to the LED-tower (red), irradiating at 405, 447, and 525 nm (see Table TS 3, entry 1) at various irradiation times.

These experiments have been restricted to the most suitable chromophore **4d**. However, for both catalysts only the best results are reported. TONs of **4d** with $[Fe_3(CO)_{12}]$ and 700W Hg irradiation (blue) and with $[Ni(py\text{-}S)_3](NEt_4)$ after exposure to LED-tower (red) at various irradiation times are shown. In the case of $[Fe_3(CO)_{12}]$ LED-irradiation shows lower TONs than with 700W Hg irradiation, and in the case of $[Ni(py\text{-}S)_3](NEt_4)$ *vice versa*. Thus a comparison is possible between the best obtained results. Furthermore, hydrogen evolution is always measured until a plateau is reached, indicating that no further hydrogen is produced. In the case of $[Fe_3(CO)_{12}]$ the plateau is reached after five measuring points, for $[Ni(py\text{-}S)_3](NEt_4)$ after three. At earlier times, the hydrogen evolution is difficult to measure, possibly as a consequence of long induction periods for catalytic activities.

References from the experiments with **4d**: The catalysts were measured without **4d** to ensure the dependence of the hydrogen production of the developed chromophore. For those references $[Ni(py\text{-}S)_3](NEt_4)$ (10.0 equiv., 2.89 µmol) and $[Fe_3(CO)_{12}]$ (20.0 equiv.; 23.5 µmol) no significant H_2 production was detected.

3.7. Comparison of mono- and tri-nuclear complexes

Table TS 6: Comparison of the TONs and conditions of mono- and trinuclear complexes.

complex	**8a [$(PdCl_2)_3$(tris(PNP-Me)benzene)]**	**8b [$(Pd(ACN)_2)_3$(tris(PNP-Me)benzene)]$(PF_6)_6$**	**[$PdCl_2$(PNP-C1-Me)]**	**[$Pd(ACN)_2$(PNP-C1-Me)]$(BF_4)_2$**
n WRC (µmol)	0.45	0.28	0.98	1.00
ratio PS:WRC	12:1	12:1	28:1	28:1
irradiation lamp	700W Hg	700W Hg	150W Hg	150W Hg
irradiation solution	15 mL solution 2	15 mL solution 2	20 mL solution 1	20 mL solution 1
time (h)	233	277	1245	1245
TON	**5154**	**8899**	**842**	**2289**

4. Crystallography.

Prior to the XRD measurements, the single crystals were handpicked using a Leica Wild M10 microscope with vertical illumination and a polarising filter. Single-crystal X-ray diffraction analysis of [(Cu(3,8-bis[3,5-bis(trifluoromethyl)phenyl]-1,10-phenanthroline)$_3$(1,3,5-tris(PNPmethylene)benzene](BF$_4$)$_3$ ·0.95diethylether·2-water·0.86acetonitrile, **4d**, was performed on a Bruker D8 diffractometer with incoatex-microfocus-channel, a multi-layer-monochromator and the new CMOS-technology from Bruker (D8 Quest). Cell refinement, data reduction and the empirical absorption correction were performed using Apex III and Saint-V 8.34 A programmes. All structure determination calculations were realised using SHELXTL-NT V6.1 and SHELXL-2014/7. Final refinements on F^2 were done with anisotropic thermal parameters for all non-hydrogen atoms in all cases except for three disordered fluorine atoms belonging to rotating trifluoromethyl groups. The hydrogen atoms were included using a riding model with isotropic *U* values depending on the U_{eq} of the adjacent carbon atoms. In the case of substantially disordered solvent molecules, the hydrogen atoms on these solvent molecules have been omitted.

Crystallographic data and refinement results are given in the Supporting Information. CCDC-2110798 (for **4d**) contains the supplementary crystallographic data for this paper. These data can be obtained free of charge from The Cambridge Crystallographic Data Centre via www.ccdc.cam.ac.uk/data_request/cif.

5. Selected NMR Spectra

All spectra were captured in deuterated solvents and referenced by the solvent signals.

1,3,5-Tris(azidomethyl)benzene ^{1}H and ^{13}C NMR

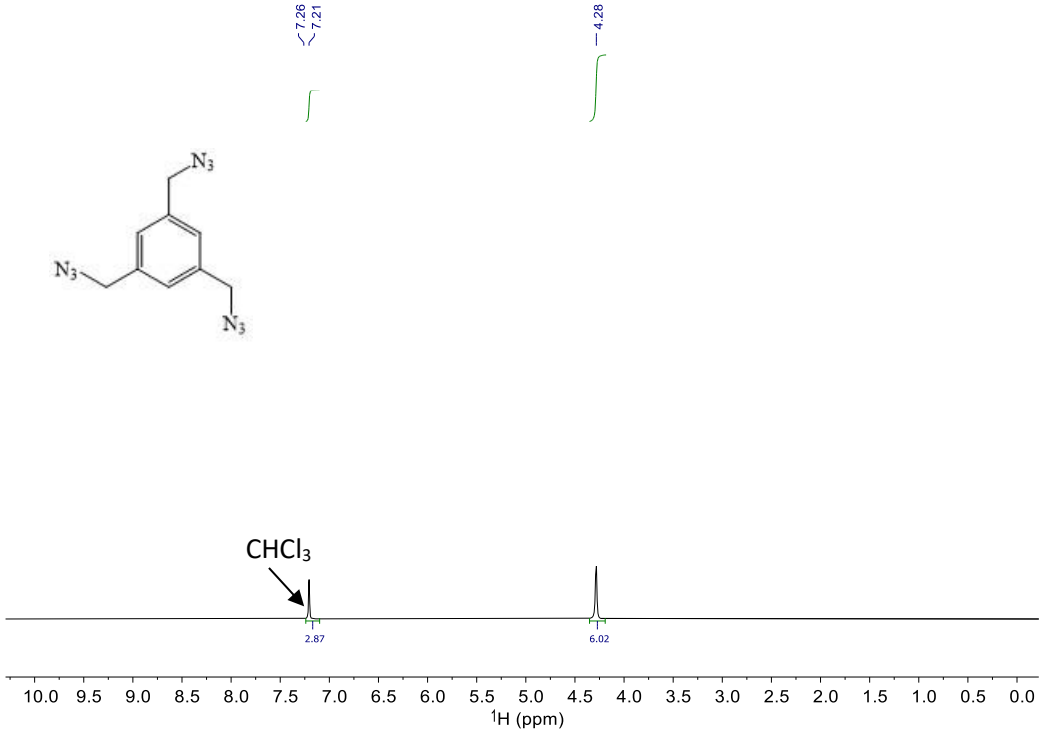

Figure S 8: ^{1}H spectrum of 1,3,5-Tris(azidomethyl)benzene in $CDCl_3$. The solvent signal overlaps next to the benzene-H peak but was excluded from integration.

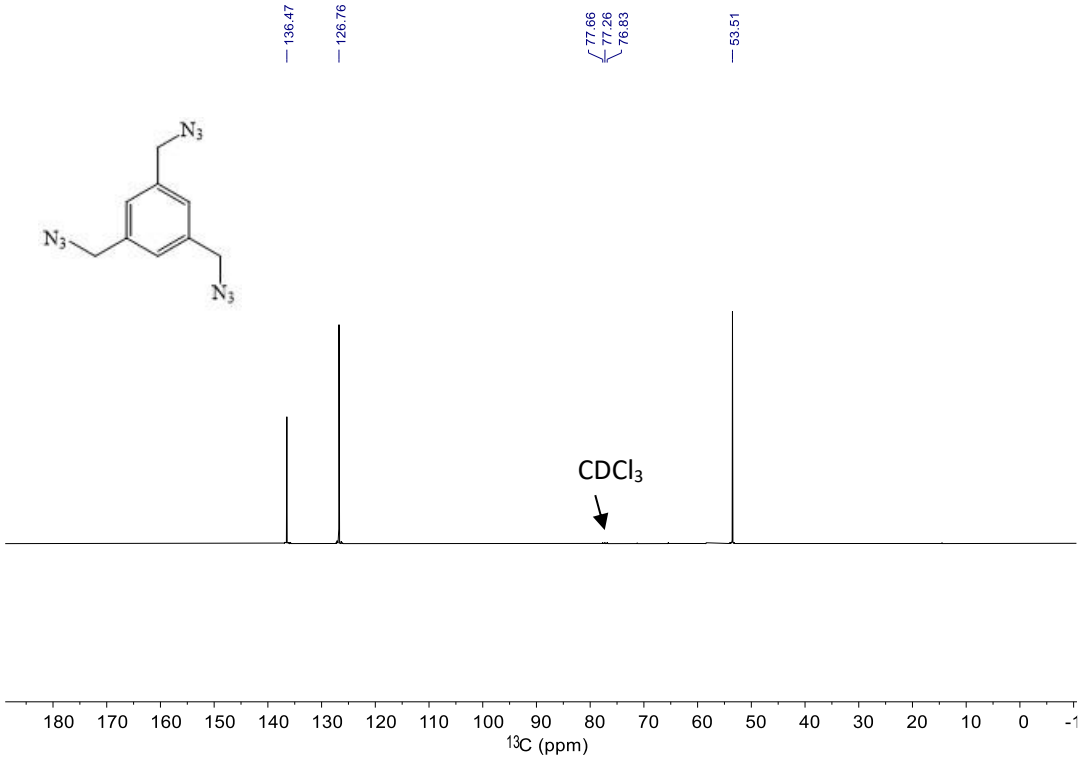

Figure S 9: ^{13}C spectrum of 1,3,5-Tris(azidomethyl)benzene in $CDCl_3$.

1,3,5-Tris(ammoniumchloridomethyl)benzene ^{1}H and ^{13}C NMR

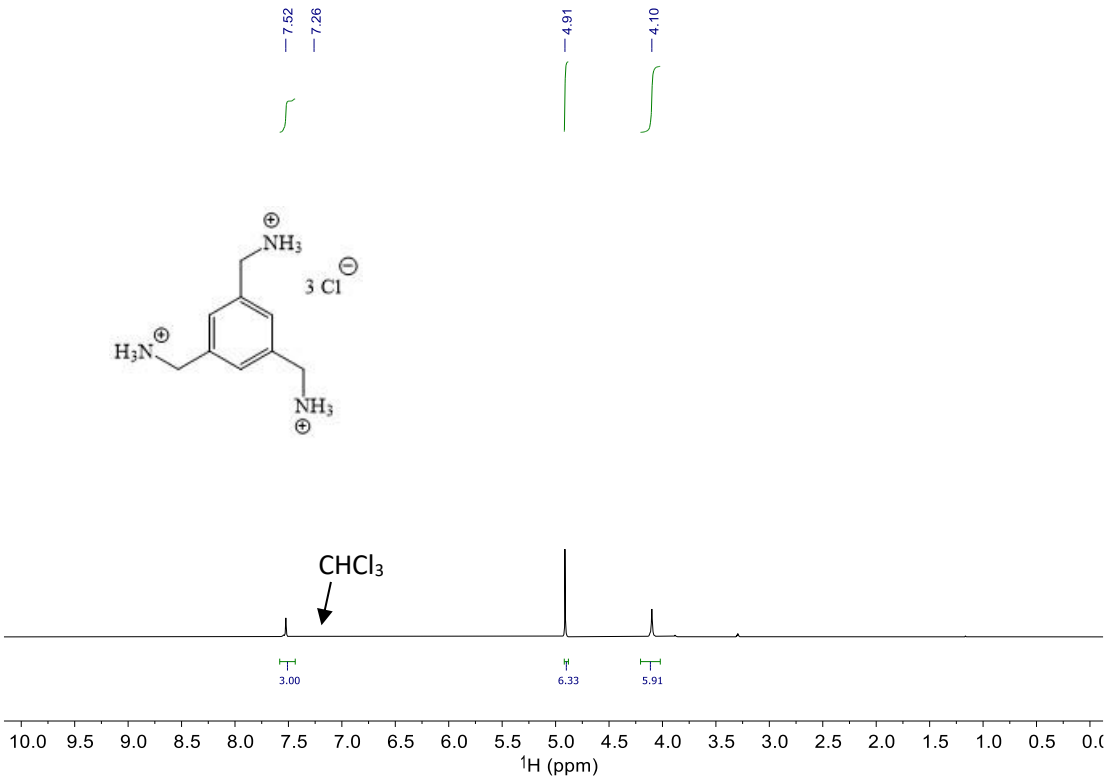

Figure S 10: ^{1}H spectrum of 1,3,5-Tris(ammoniumchloridomethyl)benzene in $CDCl_3$.

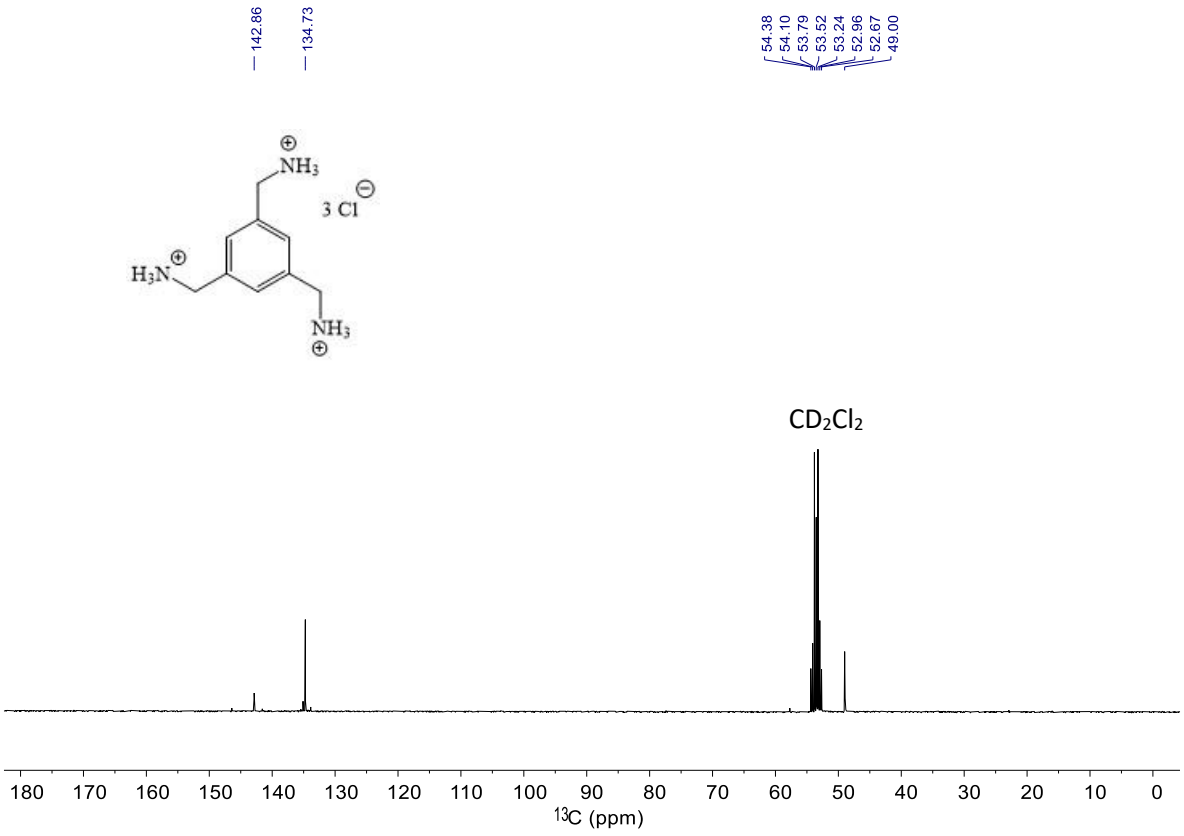

Figure S11: ^{13}C spectrum of 1,3,5-Tris(ammoniumchloridomethyl)benzene in CD_2Cl_2.

3-^{1}H NMR and ^{31}P NMR

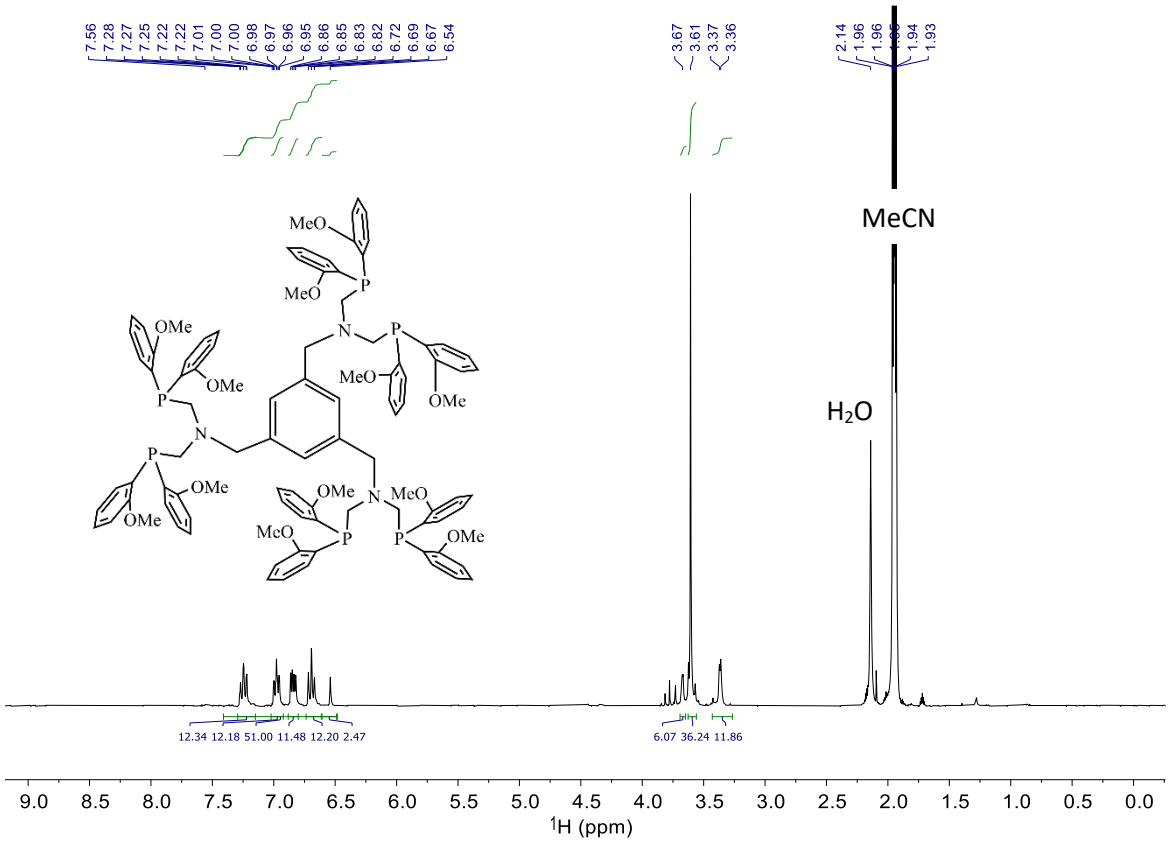

Figure S 12: ^{1}H spectrum of 1,3,5-Tris(PNP-Me)benzene (**3**) in MeCN-d_3.

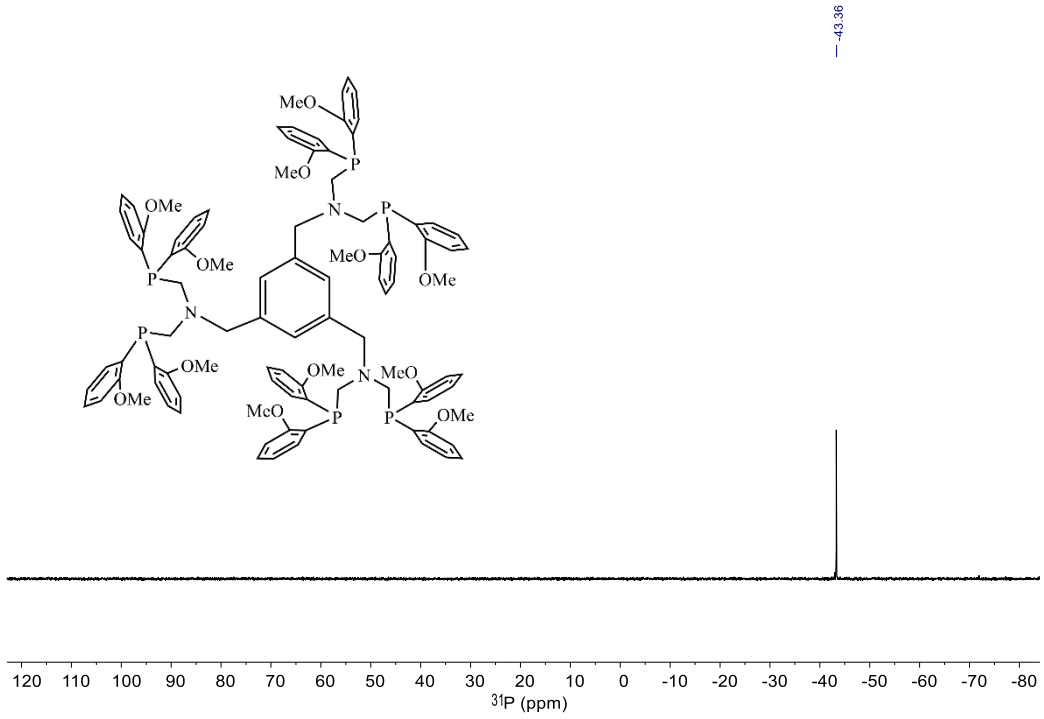

Figure S 13: ^{31}P spectrum of 1,3,5-Tris(PNP-Me)benzene (**3**) in MeCN-d_3.

4d- ^{1}H and ^{31}P NMR

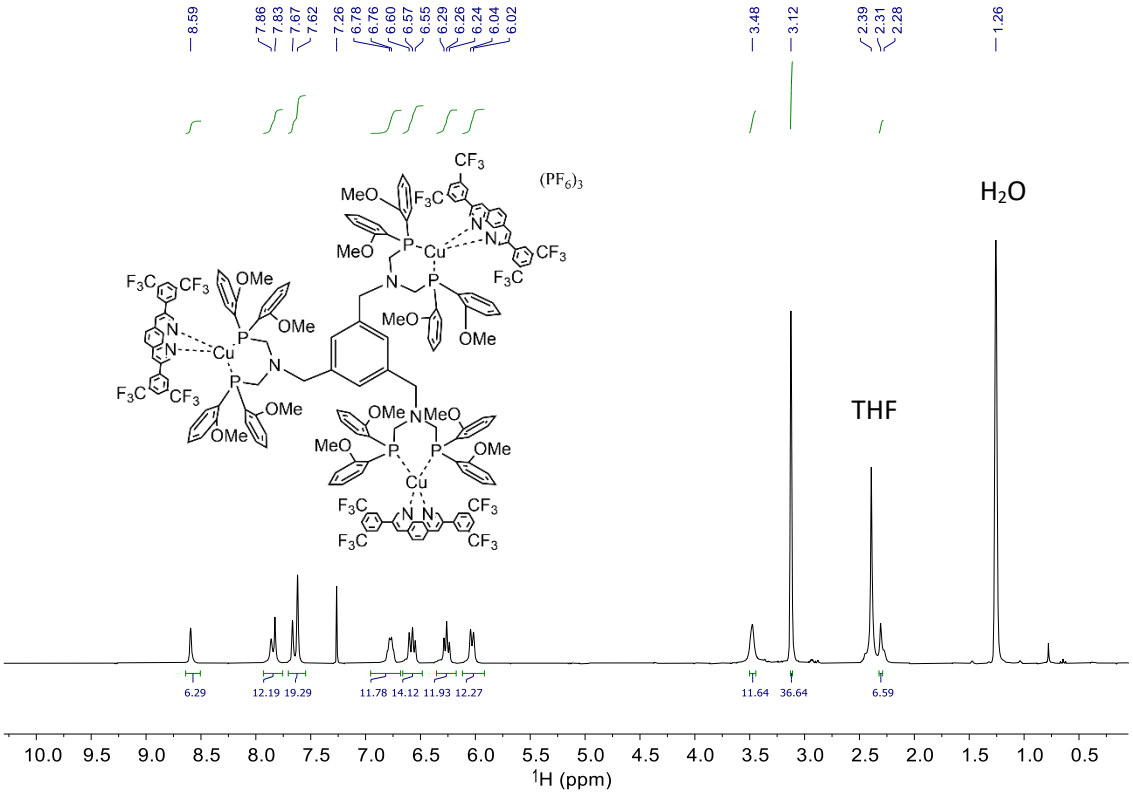

Figure S 14: ^{1}H spectrum of **4d** in $CDCl_3$/ THF-d_8 mixture.

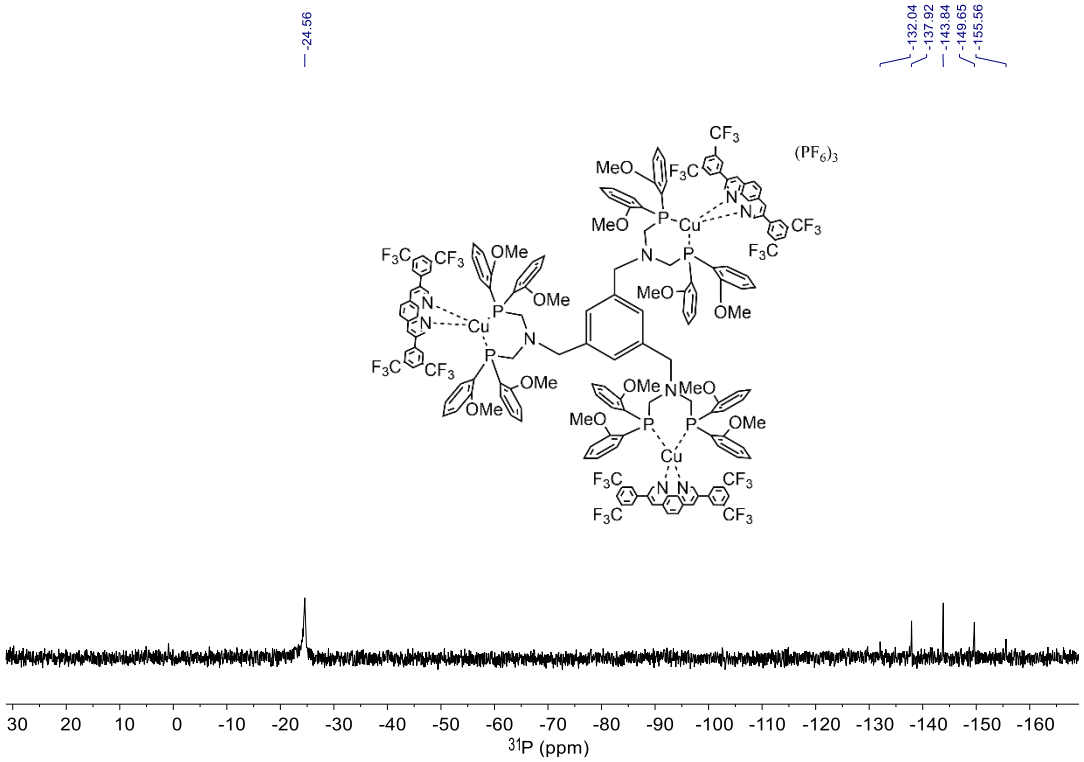

Figure S 15: ^{31}P spectrum of **4d** in $CDCl_3$/ THF-d_8 mixture.

6c-^{1}H and ^{31}P NMR

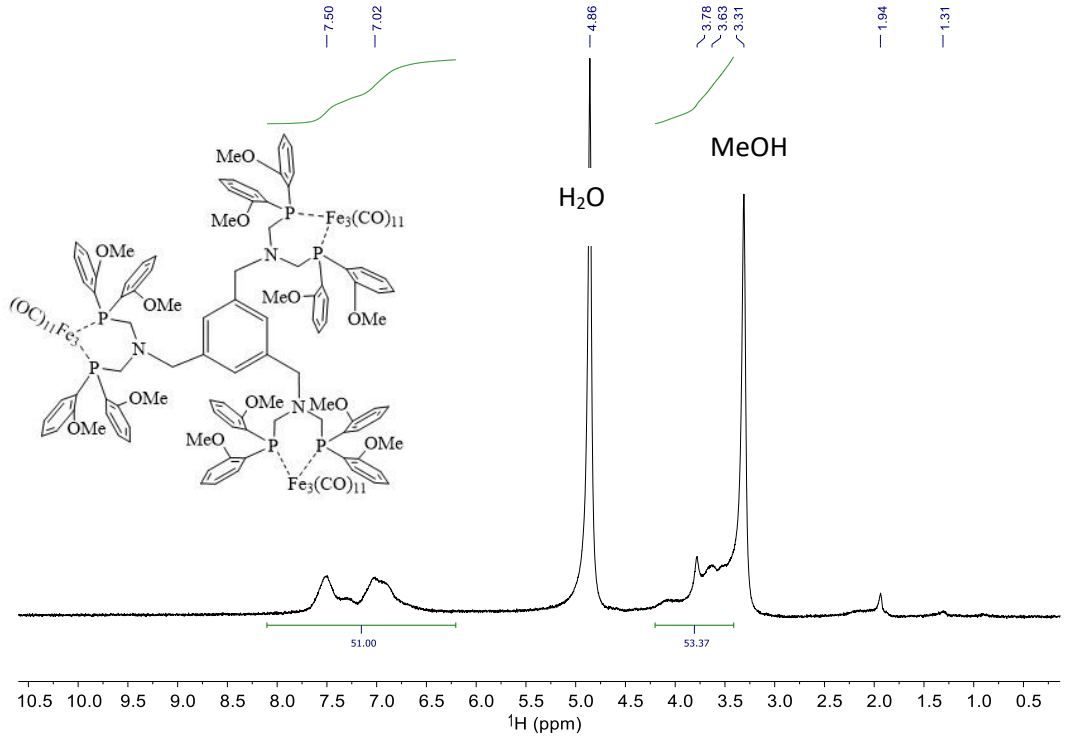

Figure S 16: ^{1}H NMR spectrum of **6c** in MeOD. Broad signals were obtained due to high spin properties.

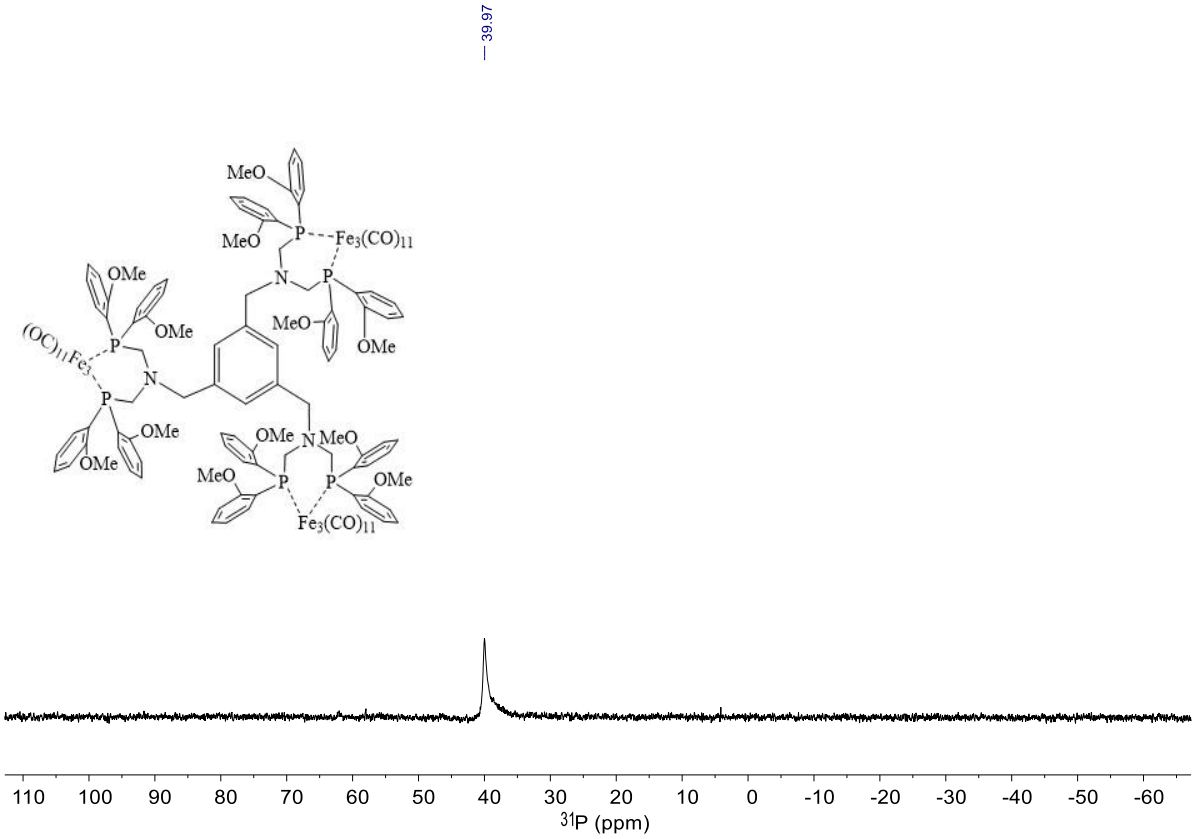

Figure S 17: ^{31}P NMR spectrum of **6c** in MeOD.

7a-^{1}H and ^{31}P NMR

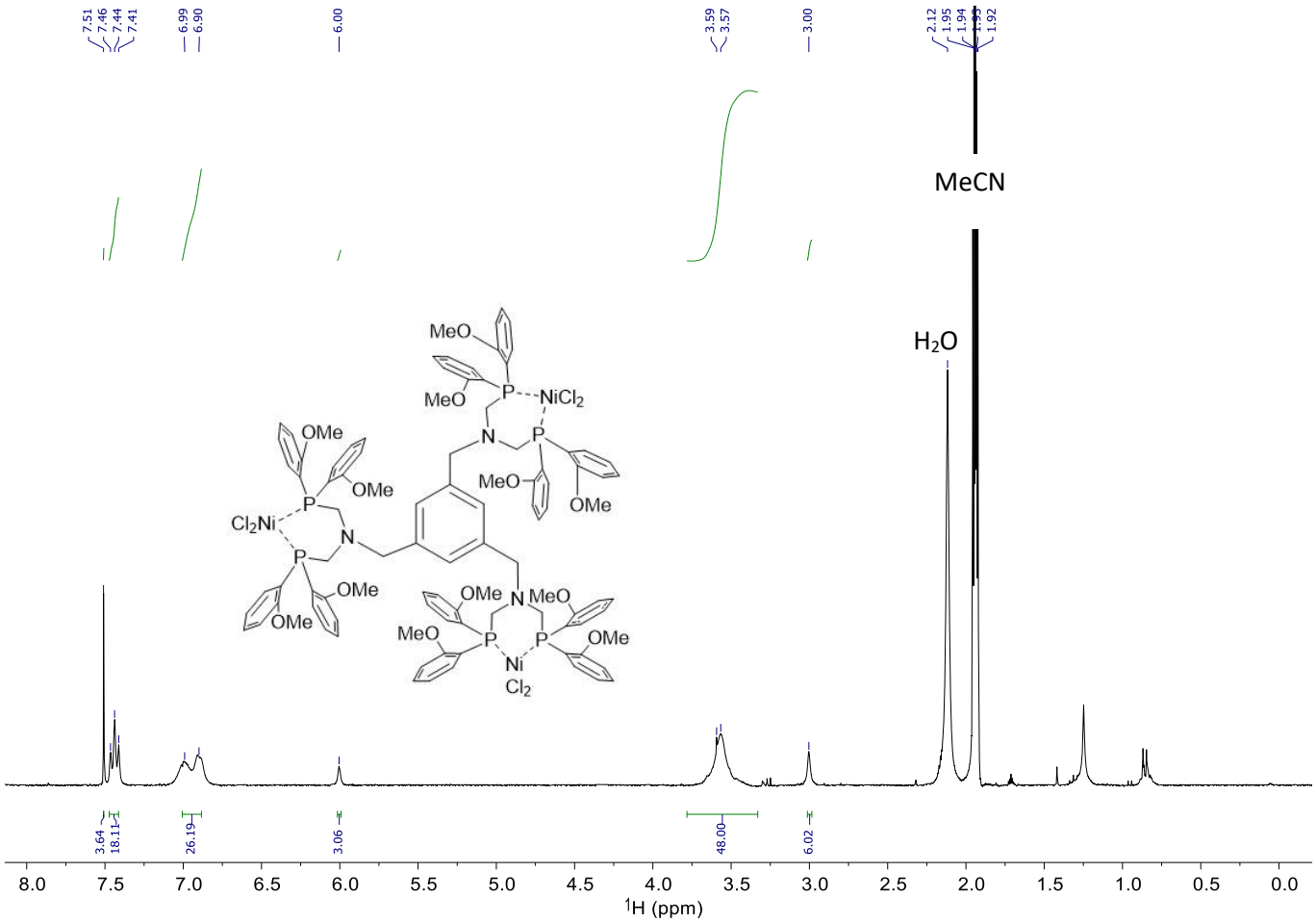

Figure S 18: ^{1}H spectrum of **7a** in MeCN-d_3.

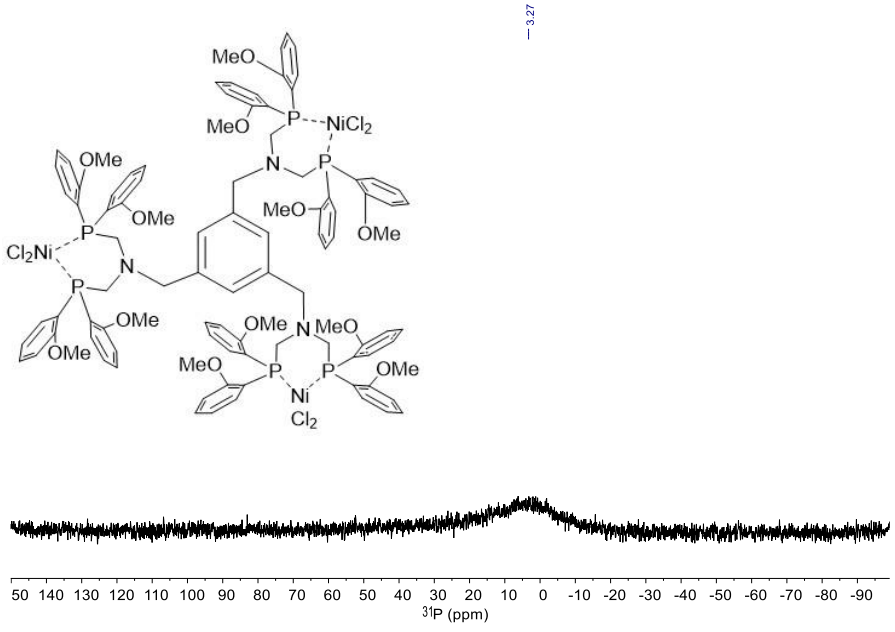

Figure S 19: ^{31}P spectrum of **7a** in MeCN-d3.

7b-^{1}H and ^{31}P NMR

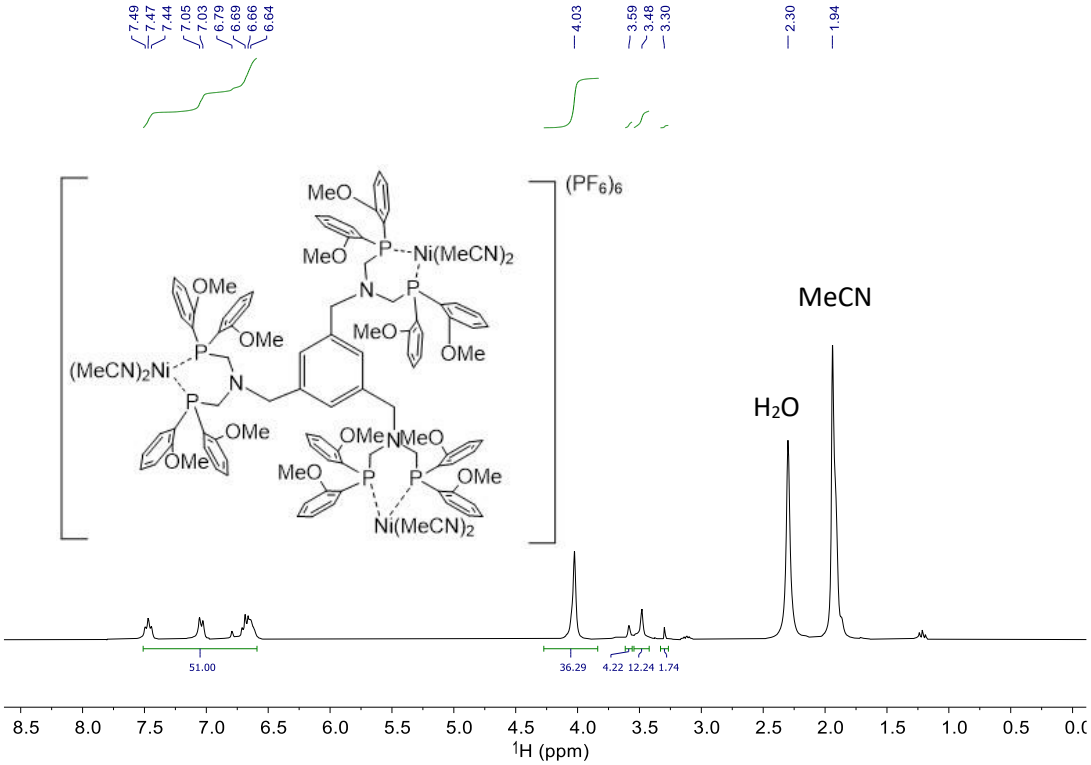

Figure S 20: ^{1}H spectrum of **7b** in MeCN-d_3.

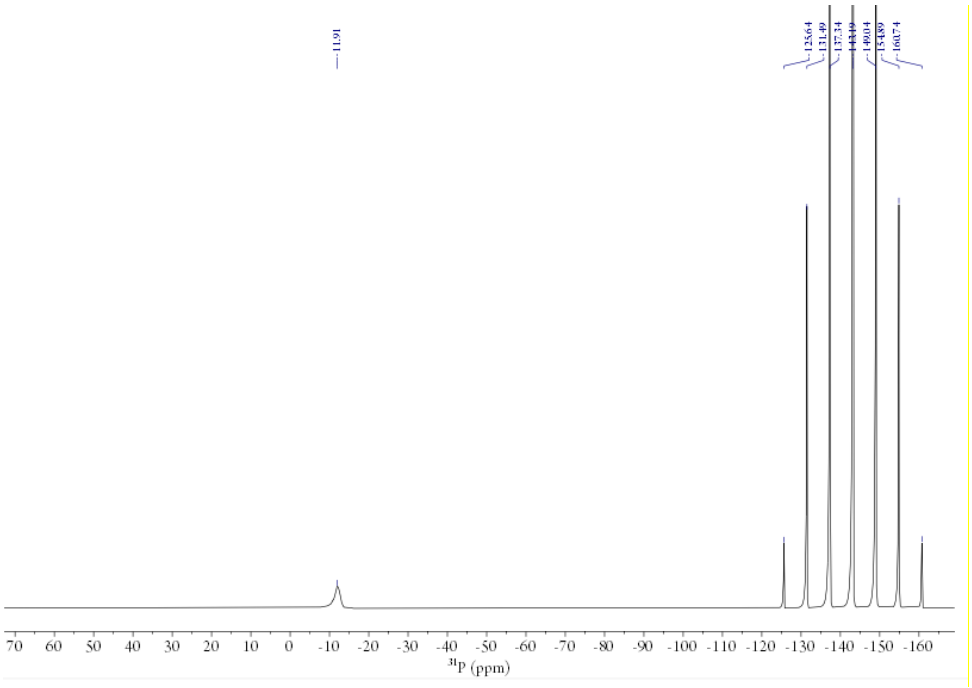

Figure S 21: ^{31}P spectrum of **7b** in MeCN-d_3.

8a-^{1}H and ^{31}P NMR

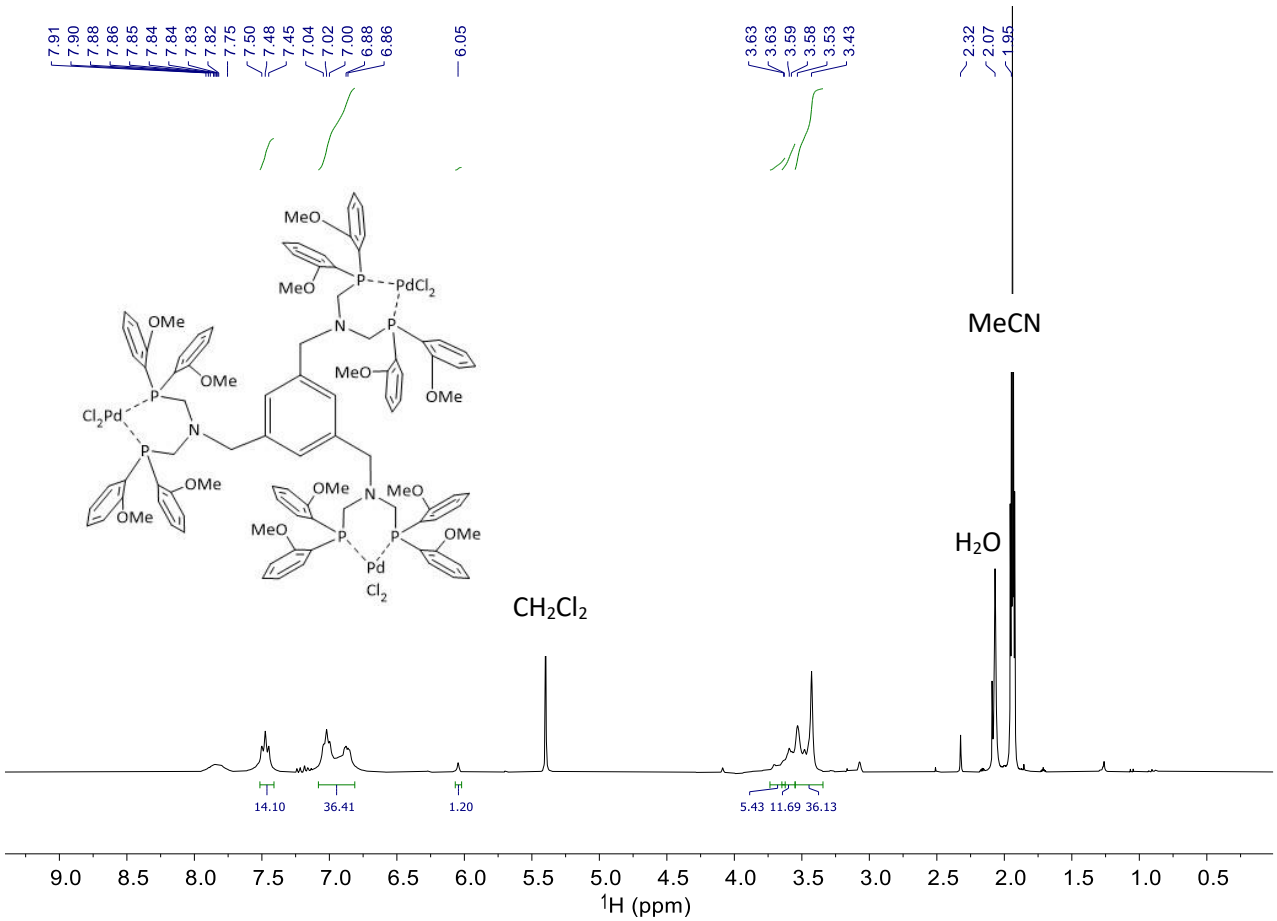

Figure S 22: ^{1}H NMR spectrum of **8a** in MeCN-d_3 and a drop of CD_2Cl_2 for better solubility.

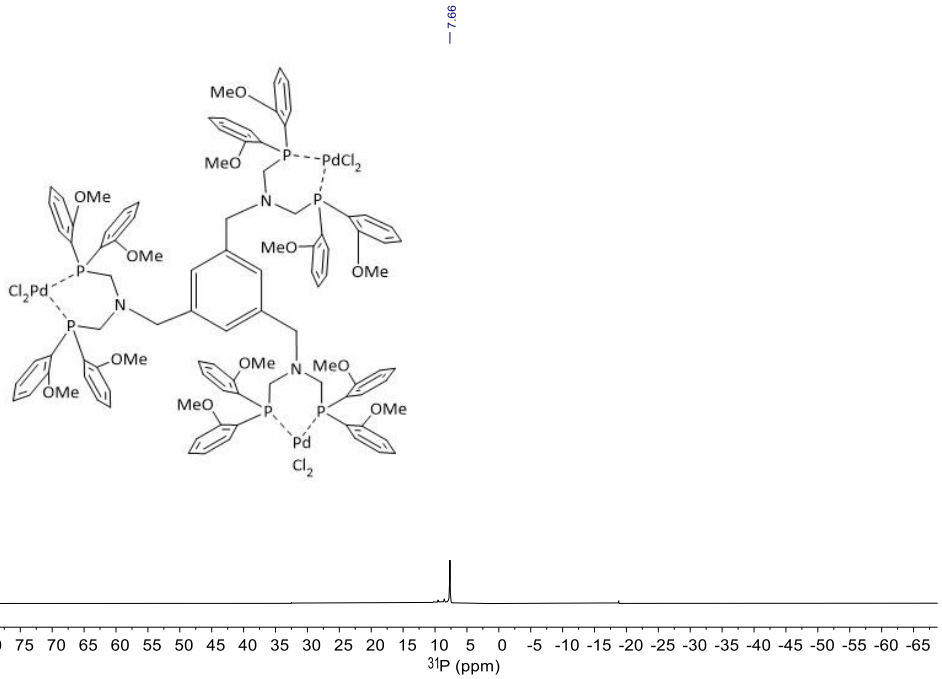

Figure S 23: ^{31}P NMR spectrum of **8a** in MeCN-d_3.

8b-^{1}H and ^{31}P NMR

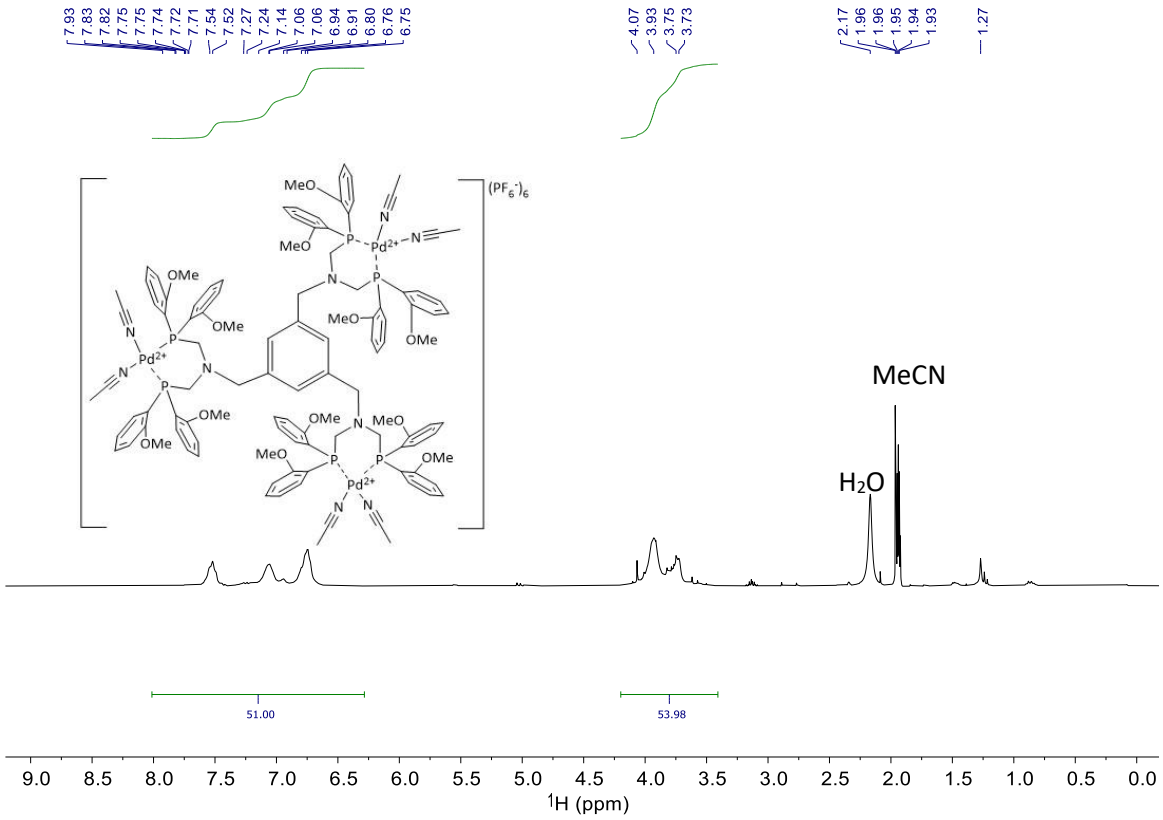

Figure S 24:^{1}H NMR spectrum of **8b** in MeCN-d_3.

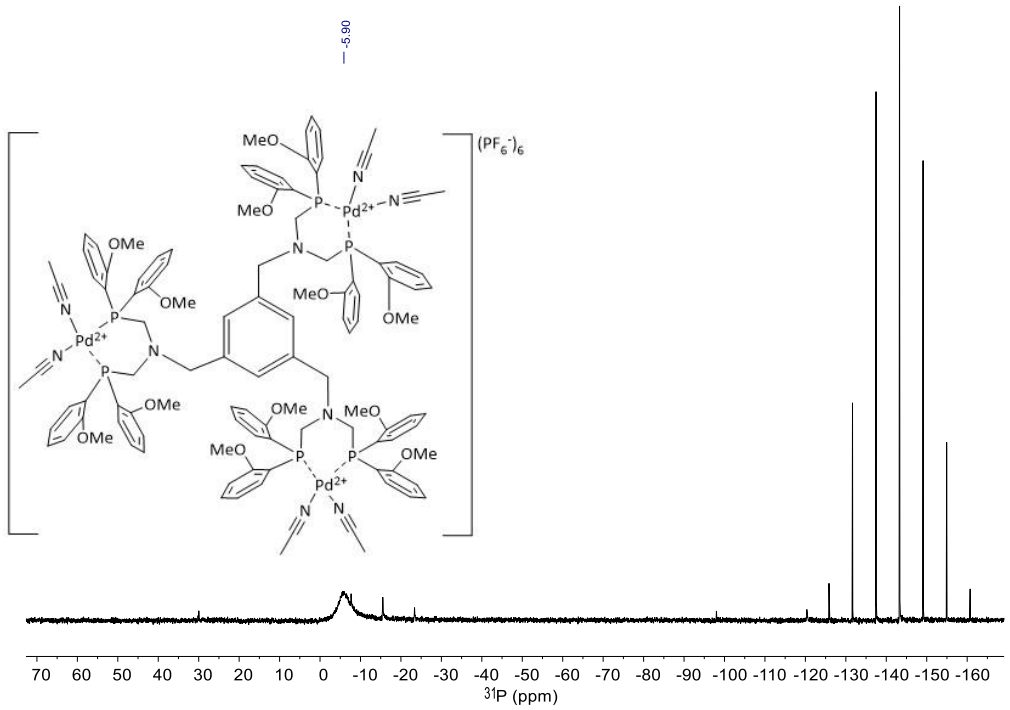

Figure S 25: ^{31}P NMR spectrum of **8b** in MeCN-d_3.

9a- ^{1}H and ^{31}P NMR

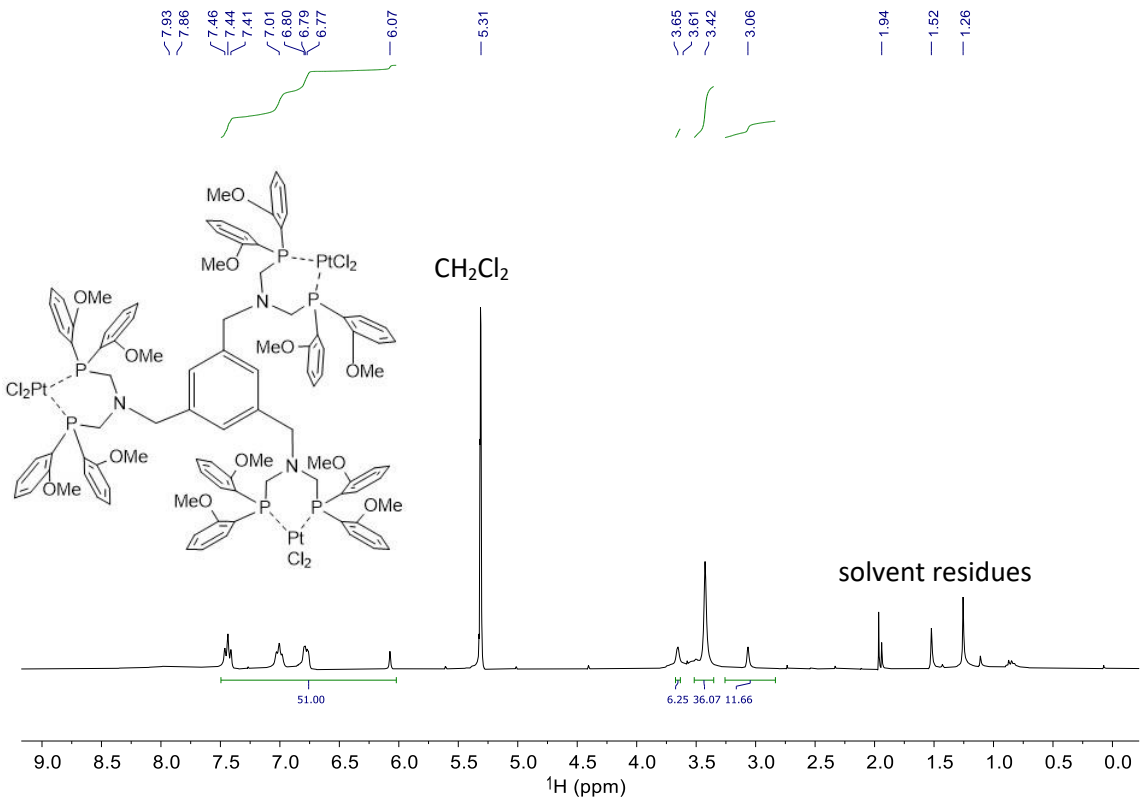

Figure S 26 : ^{1}H NMR of **9a** in CD_2Cl_2.

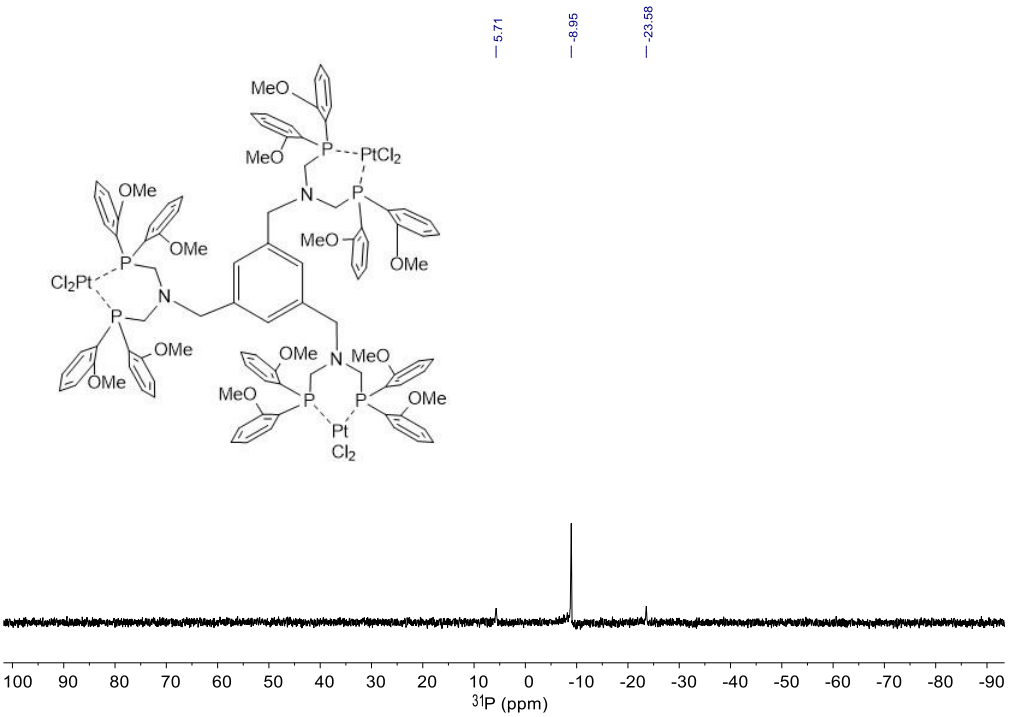

Figure S 27: ^{31}P NMR of **9a** in CD_2Cl_2.

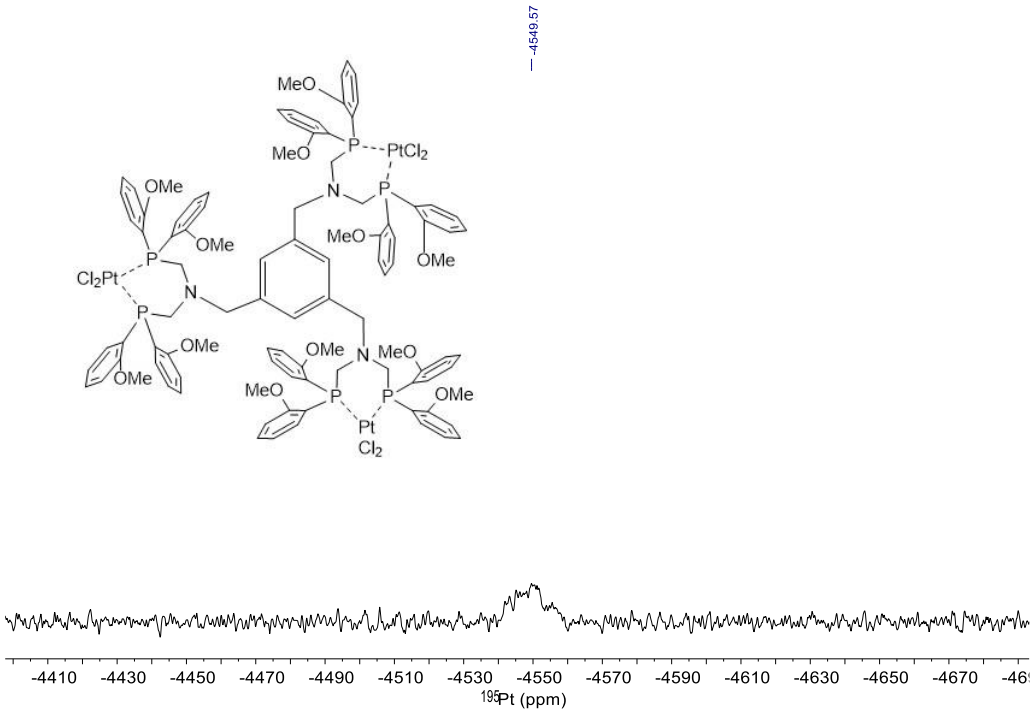

Figure S 28: ^{195}Pt NMR of **9a** in CD_2Cl_2.

9b-^{1}H and ^{31}P NMR

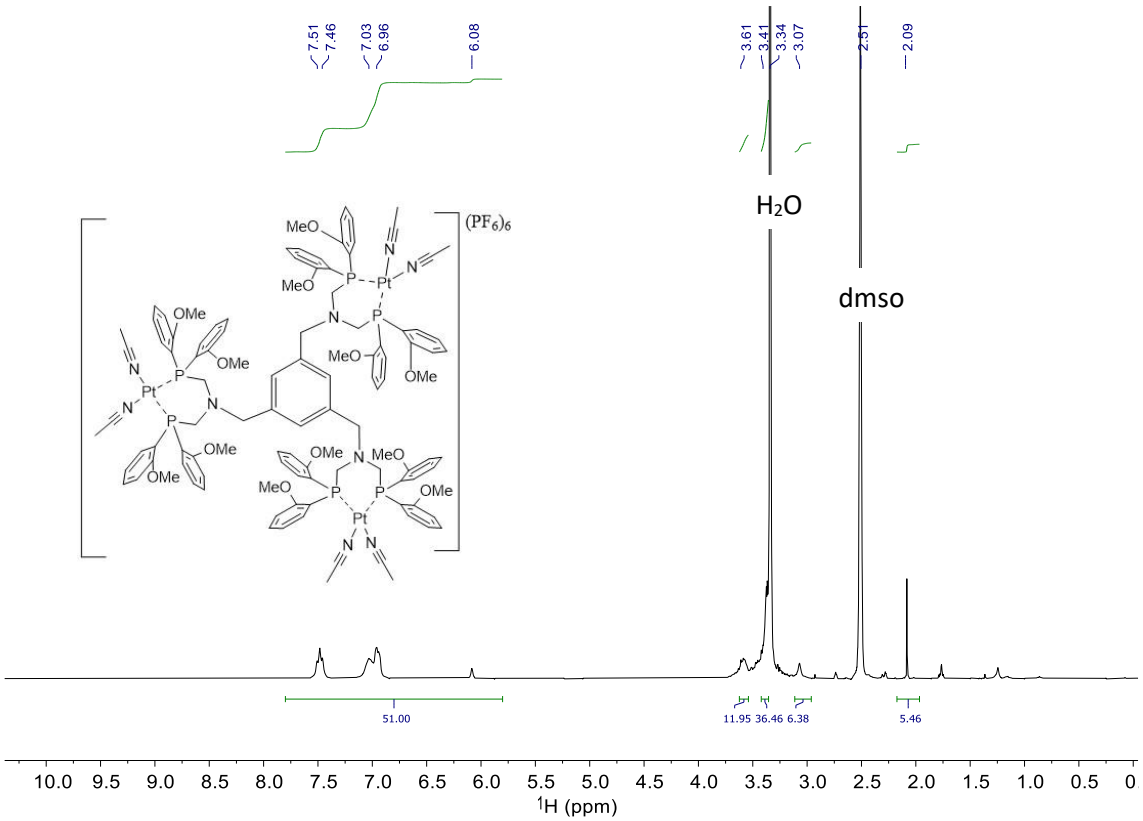

Figure S 29: ^{1}H NMR of **9b** in dmso-d_6. The methoxy peak is overlapping in the shoulder of the water solvent residual peak.

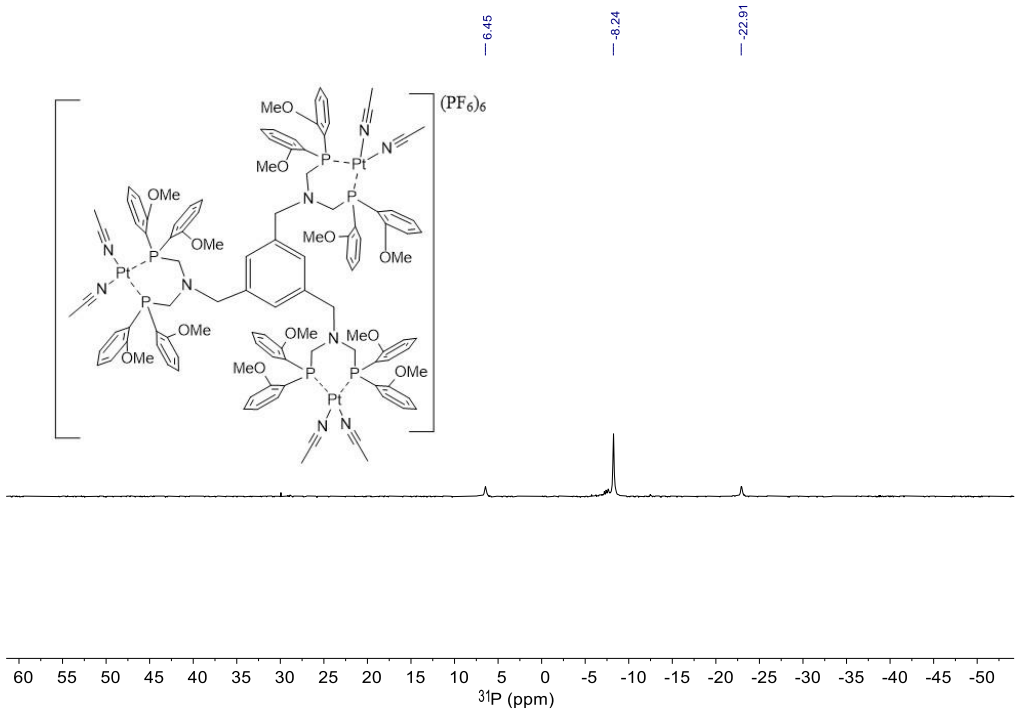

Figure S 30: ^{31}P NMR of **9b** in dmso-d_6.

6. References

1 G. Czermak, LFU, 2006.

2 A. Granzhan, C. Schouwey, T. Riis-Johannessen, R. Scopelliti and K. Severin, *J Am Chem Soc*, 2011, **133**, 7106–7115.

3 R. Pötzsch and B. Voit, *Macromol Rapid Commun*, 2012, **33**, 635–639.

4 E. Stein and F. Y. Fujiwara, *J Organomet Chem*, 1996, **525**, 31–37.

5 E. M. Simmons and J. F. Hartwig, *Angewandte Chemie International Edition*, 2012, **51**, 3066–3072.

6 H. T. Flakus, *J Mol Struct*, 2003, **646**, 15–23.

7 H. Weingärtner, *Annu. Rep. Prog. Chem., Sect. C: Phys. Chem.*, 1994, **91**, 37–69.

8 *Proc R Soc Lond A Math Phys Sci*, 1956, **235**, 518–536.

9 H. J. Kuhn, S. E. Braslavsky and R. Schmidt, *Pure and Applied Chemistry*, 2004, **76**, 2105–2146.

10 M. Nič, J. Jirát, B. Košata, A. Jenkins and A. McNaught, *The IUPAC Compendium of Chemical Terminology*, International Union of Pure and Applied Chemistry (IUPAC), Research Triangle Park, NC, 2019.

11 D. E. Nicodem and O. M. V. Aquilera, *Journal of Photochemistry*, 1983, **21**, 189–193.

12 H. Grüter, *J Appl Phys*, 1980, **51**, 5204.

13 J. N. Demas, W. D. Bowman, E. F. Zalewski and R. A. Velapoldi, *J Phys Chem*, 1981, **85**, 2766–2771.